

ELECTROMAGNETIC SCATTERING BY SIMPLE ICE  
CRYSTAL SHAPES

Richard Silveira

August 25, 2006

## Abstract

We consider the problem of electromagnetic scattering by simple ice crystal shapes. This has important meteorological applications, where understanding the behaviour of scattered radiation through clouds can enable the remote measurement of quantities such as ice crystal sizes and cloud optical depths. We solve Maxwell's equations to set up a boundary-value transmission problem. The Helmholtz equation is satisfied inside and outside the ice crystal with complex and real wavenumbers respectively. We apply Green's Representation Theorem to reformulate the problem as a set of boundary integral equations, for which the unknowns are the total field and its normal derivative. We solve via a Galerkin boundary element method, originally developed for acoustic scattering, and investigate its effectiveness. Some encouraging results are obtained, though we note the limitations of applying such a method to our problem. Further work is suggested that may alleviate these constraints.

### Acknowledgements

I would like to thank my supervisors for this project, Professor Simon Chandler-Wilde and Dr. Stephen Langdon, for their generous time and support, and everyone on the Msc course and in the Maths department who has made this year tremendously enjoyable. I would also like to acknowledge the NERC for funding this work.

### Declaration

I confirm this report is all my own work and any material taken from other sources has been fully and properly acknowledged.

Richard Silveira

## Contents

<b>1</b>	<b>Introduction</b>	<b>8</b>
<b>2</b>	<b>The Boundary-Value Transmission Problem</b>	<b>9</b>
2.1	From Maxwell's equations to the Helmholtz equation . . . . .	9
2.2	Boundary conditions . . . . .	12
2.3	Sommerfeld Radiation Condition . . . . .	12
2.4	Green's Representation Theorem . . . . .	12
2.5	Leading Order Behaviour . . . . .	16
2.5.1	Illuminated sides . . . . .	16
2.5.2	Shadow sides . . . . .	18
2.6	Modified integral equations . . . . .	19
<b>3</b>	<b>Parameterisation and the Approximation Space</b>	<b>21</b>
3.1	Parameterisation . . . . .	21
3.2	The approximation space . . . . .	23
3.2.1	The mesh and basis functions . . . . .	25
<b>4</b>	<b>The Galerkin Method</b>	<b>26</b>
4.1	Left Hand Side . . . . .	28
4.1.1	$L_1$ . . . . .	29
4.1.2	$L_2$ and $L_3$ . . . . .	29
4.1.3	$L_4$ . . . . .	31
4.1.4	$L_5$ . . . . .	33
4.2	Right Hand Side . . . . .	35
4.2.1	$R_1$ and $R_2$ . . . . .	36
4.2.2	$R_3, R_4, R_5, R_6$ . . . . .	36
4.3	Gaussian quadrature . . . . .	39

4.3.1	1-D non-oscillatory integrals . . . . .	40
4.3.2	2-D oscillatory integrals . . . . .	40
<b>5</b>	<b>Numerical Results</b>	<b>42</b>
5.1	Reproducing an acoustic scattering problem . . . . .	42
5.2	Acoustic scattering problem without subtraction of the leading order behaviour . . . . .	44
5.3	Transmission through a hexagonal ice crystal . . . . .	45
5.4	Transmission through a triangular ice crystal . . . . .	46
5.5	Transmission through a thin strip . . . . .	47
<b>6</b>	<b>Conclusions and Further Work</b>	<b>47</b>

## List of Figures

2.1	The boundary-value transmission problem . . . . .	10
2.2	Leading order behaviour of the field on an illuminated side . . . . .	17
2.3	Multiple ray contributions at a shadow side . . . . .	19
3.1	Parameterisation . . . . .	21
3.2	Diffracted behaviour at a corner . . . . .	24
4.1	Overlapping basis functions . . . . .	32
4.2	Basis functions near the same corner . . . . .	41
4.3	Graded mesh near a singularity or peak . . . . .	42
5.1	Total (left) and diffracted (right) fields for an acoustic scattering problem, $k = 4, \theta = \pi/4, N = 128$ . Original result (top), our approximation (bottom) . . . . .	43
5.2	$ \varphi $ (left) and $ \varphi_{\partial u/\partial n} $ (right) on the boundary . . . . .	44
5.3	Acoustic scattering without subtraction of leading order behaviour, $N=8,16,32,64$ . . . . .	45
5.4	Acoustic scattering with subtraction of leading order behaviour, $k=10, N=64$ . . . . .	46
5.5	Total (left) and transmitted (right) fields for transmission through a hexagon, $k = 20, \theta = 49\pi/100, N = 2, 4, 8$ . . . . .	49
5.6	Total (left) and transmitted (right) fields for transmission through a hexagon, $k = 20, \theta = 49\pi/100, N = 16, 32, 64$ . . . . .	50
5.7	Plots of $ \varphi_u $ (left) and $ \varphi_{\partial u/\partial n} $ (right) on the boundary of the hexagon . . . . .	51
5.8	Total field plotted for transmission through a triangle, $k = 4, \theta = \pi/3, N = 16$ (top left), $N = 32$ (top right), $N = 64$ (bottom left) and $N = 128$ (bottom right) . . . . .	52
5.9	Plots of $ \varphi_u $ and $ \varphi_{\partial u/\partial n} $ on the boundary of the triangle . . . . .	53
5.10	Total and transmitted fields for transmission through a thin strip . . . . .	53

## List of Tables

5.1	Relative L2 errors for acoustic case where there is no subtraction . . . . .	44
5.2	Relative L2 errors for triangle case . . . . .	51

## 1 Introduction

Electromagnetic scattering is an important application in many areas of science and industry, from the modelling of an optical security device to x-ray diffraction. Acoustic scattering is an analogous field on which there is considerable literature. Therefore any novel techniques that arise in one field may have a useful purpose in the other.

The aim of this dissertation is to investigate the extent to which the numerical solution of electromagnetic scattering problems can be enhanced using methods developed for acoustic scattering. In particular we employ a Galerkin boundary element method which incorporates the product of plane waves with piecewise polynomials into the approximation space (see [6]).

In chapter 2 we outline the transmission problem and reformulate it as a set of integral equations on the boundary, then we investigate the leading order behaviour and modify the integral equations accordingly.

In chapter 3 we parameterise the problem on the boundary and define the approximation space.

In chapter 4 we set up the linear system, and proceed to give an in depth description of how we evaluate the matrix entries.

In chapter 5 we conduct a variety of numerical experiments to test our method. We have no error analysis or test data against which to check (with the exception of the original acoustic scattering problem), so we rely on a qualitative check for convergence

We conclude by giving an overview of the project and suggesting ways in which the work can be carried forward.

## 2 The Boundary-Value Transmission Problem

### 2.1 From Maxwell's equations to the Helmholtz equation

We start with Maxwell's equations, which describe the propagation of electromagnetic waves in a medium.

$$\begin{aligned}\nabla \cdot E &= \frac{\rho}{\epsilon} \\ \nabla \cdot H &= 0 \\ \nabla \times E + \mu \frac{\partial H}{\partial t} &= 0 \\ \nabla \times H - \epsilon \frac{\partial E}{\partial t} - \sigma E &= 0\end{aligned}$$

where  $\sigma$  is the electric conductivity,  $\mu$  is the magnetic permeability,  $\epsilon$  is the electric permittivity and  $\rho$  is the charge density, all properties of the medium. We consider the medium to be homogeneous and isotropic, where the above parameters are constant, and describe the time harmonic electric and magnetic fields by

$$E(\mathbf{x}, t) = \operatorname{Re} [E(\mathbf{x})e^{-i\omega t}]$$

$$H(\mathbf{x}, t) = \operatorname{Re} [H(\mathbf{x})e^{-i\omega t}]$$

The time-dependent equations become

$$\begin{aligned}\nabla \times E - i\omega\mu H &= 0 \\ \nabla \times H + i\omega\epsilon E - \sigma E &= 0\end{aligned}$$

Using the vector identity  $\Delta E = \nabla(\nabla \cdot E) - \nabla \times \nabla \times E$ , and noting that  $\nabla(\nabla \cdot E) = \frac{1}{\epsilon}\nabla\rho = 0$ , we see

that  $E(\mathbf{x})$  and  $H(\mathbf{x})$  satisfy the vector Helmholtz equation with wavenumber  $k$ , where  $k^2 = \omega^2\mu\epsilon + i\mu\sigma\omega$ .

$$\Delta E(\mathbf{x}) + k^2 E(\mathbf{x}) = 0$$

$$\Delta H(\mathbf{x}) + k^2 H(\mathbf{x}) = 0$$

Since the electric and magnetic fields satisfy the Helmholtz equation with the same wavenumber, we will only consider the electric field, and denote it by  $u(\mathbf{x}) = E(\mathbf{x})$ . We consider an incident electric field  $u^i(\mathbf{x})$  upon a constant cross-section ice crystal with boundary  $\Gamma$ . The ice crystal is oriented at 90 degrees to the incident wave, hence the problem is confined to a plane and is 2-D in nature.

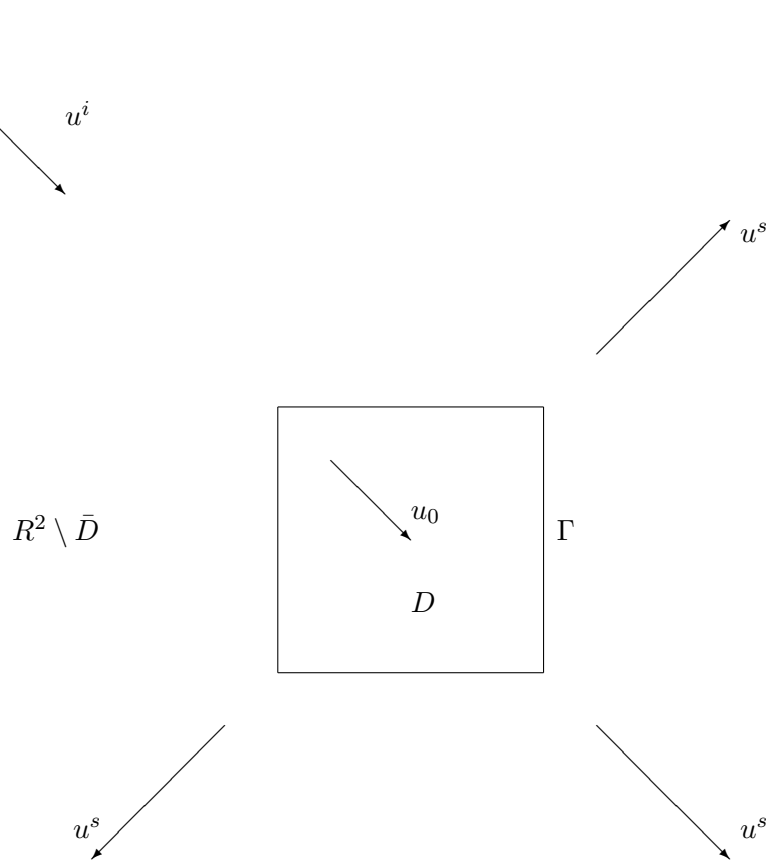


Figure 2.1: The boundary-value transmission problem

We denote the domain of the scatterer in the plane of incidence by  $D$ , with the exterior domain  $R^2 \setminus \bar{D}$ . The total field outside is given by  $u^t(\mathbf{x}) = u^i(\mathbf{x}) + u^s(\mathbf{x})$ , where  $u^s(\mathbf{x})$  is the scattered field. Inside the total field is equal to the transmitted field,  $u_0(\mathbf{x})$ . Outside we take the parameter values as those for a vacuum, which is a good approximation for air. Therefore we have  $\sigma = 0$ ,  $\epsilon = \epsilon_0$  (electric permittivity of free space) and  $\mu = \mu_0$  (magnetic permeability of free space). Inside, we take  $\mu = \mu_0$ , since ice is non-magnetic, with  $\sigma$  and  $\epsilon$  taking the appropriate values for ice (we will continue to denote by  $\sigma$  and  $\mu$  for clarity). Thus we have the scattered and transmitted fields satisfying the Helmholtz equation in both domains.

$$\Delta u^s(\mathbf{x}) + k^2 u^s(\mathbf{x}) = 0, \quad k^2 = \omega^2 \mu_0 \epsilon_0 \quad (2.1)$$

$$\Delta u_0(\mathbf{x}) + k_0^2 u_0(\mathbf{x}) = 0, \quad k_0^2 = \omega^2 \mu_0 \epsilon + i \mu_0 \sigma \omega \quad (2.2)$$

The significance of the complex wavenumber is that the transmitted field decays inside  $D$ , due to the non-zero conductivity. In the limit  $\sigma \rightarrow \infty$  (a perfect conductor), the electric and magnetic fields tend to zero as the solutions to Maxwell's equations, and the boundary-value transmission problem becomes an exterior scattering problem with Dirichlet boundary conditions ( $u^t = 0$  on  $\Gamma$ ) that is generically identical to the acoustic scattering problem in [6].

Electromagnetic radiation is generally refracted to some extent when passing between two media. The exception is when total internal reflection occurs (see 2.7). The amount of refraction is determined by the the refractive index of each medium,  $n_i$ , which is equal to the ratio of the speed of light,  $c$ , to the phase velocity in the medium,  $c_i$ , so  $n_i = c/c_i$ . Since  $c$  is constant, we have that  $n_i c_i$  is constant. We also have that the phase velocity is related to the wavenumber,  $k_i$ , by  $c_i = \omega/k_i$  (where  $\omega$  is the angular frequency and is the same in both media). For two media, denoted by subscripts 1 and 2

$$n_1 c_1 = n_2 c_2 \Rightarrow \frac{n_2}{n_1} = \frac{c_1}{c_2} = \frac{\omega/k_1}{\omega/k_2} = \frac{k_2}{k_1}$$

Thus, the ratio of the refractive indices is equal to the ratio of the wavenumbers. For our ice crystal

problem we have  $n_{ice} \approx 1.31 + 0.01i$  [3] and  $n_{air} \approx 1$ . Therefore in our notation,  $k_0/k = n_{ice}/n_{air} = 1.31 + 0.01i$ , so  $k_0 = 1.31k + 0.01ki$  for the incident wavenumber we choose.

## 2.2 Boundary conditions

We consider the TE polarisation mode, where the electric field is parallel to the boundary of  $\Gamma$ . Continuity of Maxwell's equations requires that the electric field and its normal derivative are continuous across  $\Gamma$

$$\begin{aligned} u^t &= u_0 & \text{on } \Gamma \\ \frac{\partial u^t}{\partial n} &= \frac{\partial u_0}{\partial n} & \text{on } \Gamma \end{aligned}$$

where  $n$  is the unit normal on  $\Gamma$ .

## 2.3 Sommerfeld Radiation Condition

The exterior domain is unbounded and we require to know how the scattered field, that part of the field that travels away from the scatterer, behaves as it travels outwards towards  $\infty$ . The condition we impose is called the Sommerfeld Radiation Condition (SRC), which ensures that the solution to our integral equation is unique. The SRC is

$$\lim_{r \rightarrow \infty} \left( \frac{\partial u^s}{\partial r}(\mathbf{x}) - iku^s(\mathbf{x}) \right) = 0$$

where  $r = |\mathbf{x}|$  and the limit holds uniformly in all directions  $\mathbf{x}/|\mathbf{x}|$ .

## 2.4 Green's Representation Theorem

We have from [5, theorem 3.40] that the solution to the transmission problem is unique. We use the representation theorems [5, theorems 3.1, 3.3] for the solutions  $u^s$  and  $u_0$ , in  $D$  and  $R^2 \setminus \bar{D}$  respectively.

$$\begin{aligned}
-u_0(\mathbf{x}) &= \int_{\Gamma} \left[ u_0(\mathbf{y}) \frac{\partial \Phi(k_0, \mathbf{x}, \mathbf{y})}{\partial \mathbf{n}(\mathbf{y})} - \frac{\partial u_0(\mathbf{y})}{\partial \mathbf{n}} \Phi(k_0, \mathbf{x}, \mathbf{y}) \right] ds(\mathbf{y}) \\
&= \int_{\Gamma} \left[ u^t(\mathbf{y}) \frac{\partial \Phi_0(\mathbf{x}, \mathbf{y})}{\partial \mathbf{n}(\mathbf{y})} - \frac{\partial u^t(\mathbf{y})}{\partial \mathbf{n}} \Phi(k_0, \mathbf{x}, \mathbf{y}) \right] ds(\mathbf{y}), \quad \mathbf{x} \in D
\end{aligned} \tag{2.3}$$

$$u^s(\mathbf{x}) = \int_{\Gamma} \left[ u^s(\mathbf{y}) \frac{\partial \Phi(k, \mathbf{x}, \mathbf{y})}{\partial \mathbf{n}(\mathbf{y})} - \frac{\partial u^s(\mathbf{y})}{\partial \mathbf{n}} \Phi(k, \mathbf{x}, \mathbf{y}) \right] ds(\mathbf{y}), \quad \mathbf{x} \in R^2 \setminus \bar{D} \tag{2.4}$$

In (2.3) we have used the boundary condition that  $u^t = u_0$  on  $\Gamma$ .  $\Phi(k, \mathbf{x}, \mathbf{y})$  and  $\Phi(k_0, \mathbf{x}, \mathbf{y})$  are the fundamental solutions to the 2-D Helmholtz equations (2.1) and (2.2)

$$\begin{aligned}
\Phi(k, \mathbf{x}, \mathbf{y}) &:= \frac{i}{4} H_0^{(1)}(k|\mathbf{x} - \mathbf{y}|) \\
\Phi(k_0, \mathbf{x}, \mathbf{y}) &:= \frac{i}{4} H_0^{(1)}(k_0|\mathbf{x} - \mathbf{y}|)
\end{aligned}$$

$H_0^{(1)}(z)$  is the Hankel function of the first kind of order zero. An important feature to note that is that as  $z \rightarrow 0$ ,  $H_0^{(1)}(z) \rightarrow -\infty * i$  and is undefined at the origin. This is relevant to some of the integrals we encounter later. We choose to solve for the total field outside,  $u^t$ , rather than the scattered field  $u^s$ . The reason for this is that if we solve for the scattered field we are left with a singular integral, whereas if we consider the total field, we obtain two such terms whose singularities are equal and opposite and cancel each other out (see (4.7)). We therefore add the following term to both sides of (2.4),

$$u^i(\mathbf{x}) = \int_{\Gamma} \left[ u^i(\mathbf{y}) \frac{\partial \Phi(k, \mathbf{x}, \mathbf{y})}{\partial \mathbf{n}(\mathbf{y})} - \frac{\partial u^i(\mathbf{y})}{\partial \mathbf{n}} \Phi(k, \mathbf{x}, \mathbf{y}) \right] ds(\mathbf{y}) + u^i(\mathbf{x}), \quad \mathbf{x} \in R^2 \setminus \bar{D}$$

We then have

$$u^t(\mathbf{x}) = \int_{\Gamma} \left[ u^t(\mathbf{y}) \frac{\partial \Phi(k, \mathbf{x}, \mathbf{y})}{\partial \mathbf{n}(\mathbf{y})} - \frac{\partial u^t(\mathbf{y})}{\partial \mathbf{n}} \Phi(k, \mathbf{x}, \mathbf{y}) \right] ds(\mathbf{y}) + u^i(\mathbf{x}), \quad \mathbf{x} \in R^2 \setminus \bar{D} \tag{2.5}$$

Now let  $\mathbf{x} \rightarrow \Gamma$  and use [5, theorem 2.13] to continuously extend the double-layer potential from  $D \rightarrow \bar{D}$  and from  $R^2 \setminus \bar{D} \rightarrow R^2 \setminus D$ . The limiting values give

$$\begin{aligned}
-u_0(\mathbf{x}) &= \int_{\Gamma} \left[ u_0(\mathbf{y}) \frac{\partial \Phi(k_0, \mathbf{x}, \mathbf{y})}{\partial \mathbf{n}(\mathbf{y})} - \frac{\partial u_0(\mathbf{y})}{\partial \mathbf{n}} \Phi(k_0, \mathbf{x}, \mathbf{y}) \right] ds(\mathbf{y}) - \frac{1}{2} u_0(\mathbf{x}), \quad \mathbf{x} \in \Gamma \\
u^t(\mathbf{x}) &= \int_{\Gamma} \left[ u^t(\mathbf{y}) \frac{\partial \Phi(k, \mathbf{x}, \mathbf{y})}{\partial \mathbf{n}(\mathbf{y})} - \frac{\partial u^t(\mathbf{y})}{\partial \mathbf{n}} \Phi(k, \mathbf{x}, \mathbf{y}) \right] ds(\mathbf{y}) + \frac{1}{2} u^t(\mathbf{x}) + u^i(\mathbf{x}), \quad \mathbf{x} \in \Gamma
\end{aligned}$$

Now consider the normal derivative of (2.3) and (2.5) in the limit  $\mathbf{x} \rightarrow \Gamma$ . We use [5, theorems 2.19, 2.21] to compute separately the normal derivative of the single and double-layer potentials moving from  $D \rightarrow \bar{D}$  and from  $R^2 \setminus \bar{D} \rightarrow R^2 \setminus D$ .

$$\begin{aligned}
-\frac{\partial u_0(\mathbf{x})}{\partial \mathbf{n}} &= \frac{\partial}{\partial \mathbf{n}(\mathbf{x})} \int_{\Gamma} u_0(\mathbf{y}) \frac{\partial \Phi(k_0, \mathbf{x}, \mathbf{y})}{\partial \mathbf{n}(\mathbf{y})} ds(\mathbf{y}) - \left[ \int_{\Gamma} \frac{\partial u_0(\mathbf{y})}{\partial \mathbf{n}} \frac{\partial \Phi(k_0, \mathbf{x}, \mathbf{y})}{\partial \mathbf{n}(\mathbf{x})} ds(\mathbf{y}) + \frac{1}{2} \frac{\partial u_0(\mathbf{x})}{\partial \mathbf{n}} \right], \quad \mathbf{x} \in \Gamma \\
\frac{\partial u^t(\mathbf{x})}{\partial \mathbf{n}} &= \frac{\partial}{\partial \mathbf{n}(\mathbf{x})} \int_{\Gamma} u^t(\mathbf{y}) \frac{\partial \Phi(k, \mathbf{x}, \mathbf{y})}{\partial \mathbf{n}(\mathbf{y})} ds(\mathbf{y}) + \left[ \int_{\Gamma} \frac{\partial u^t(\mathbf{y})}{\partial \mathbf{n}} \frac{\partial \Phi(k, \mathbf{x}, \mathbf{y})}{\partial \mathbf{n}(\mathbf{x})} ds(\mathbf{y}) - \frac{1}{2} \frac{\partial u^t(\mathbf{x})}{\partial \mathbf{n}} \right] + \frac{\partial u^i(\mathbf{x})}{\partial \mathbf{n}}, \quad \mathbf{x} \in \Gamma
\end{aligned}$$

The above integral equations can be expressed in a shorter form,

$$-u + Ku - S \frac{\partial u}{\partial n} = -2u^i \quad (2.6)$$

$$-\frac{\partial u}{\partial n} + Tu - K' \frac{\partial u}{\partial n} = -2 \frac{\partial u^i}{\partial n} \quad (2.7)$$

$$u_0 + K_0 u_0 - S_0 \frac{\partial u_0}{\partial n} = 0 \quad (2.8)$$

$$\frac{\partial u_0}{\partial n} + T_0 u_0 - K'_0 \frac{\partial u_0}{\partial n} = 0 \quad (2.9)$$

where  $S, S_0, K, K_0, K', K'_0, T$  and  $T_0$  are integral operators, and for  $\psi \in L_2(\Gamma)$

$$\begin{aligned}
S\psi(\mathbf{x}) &:= \int_{\Gamma} \psi(\mathbf{y})\Phi(k, \mathbf{x}, \mathbf{y})ds(\mathbf{y}) \\
S_0\psi(\mathbf{x}) &:= \int_{\Gamma} \psi(\mathbf{y})\Phi(k_0, \mathbf{x}, \mathbf{y})ds(\mathbf{y}) \\
K\psi(\mathbf{x}) &:= \int_{\Gamma} \psi(\mathbf{y})\frac{\partial\Phi(k, \mathbf{x}, \mathbf{y})}{\partial\mathbf{n}(\mathbf{y})}ds(\mathbf{y}) \\
K_0\psi(\mathbf{x}) &:= \int_{\Gamma} \psi(\mathbf{y})\frac{\partial\Phi(k_0, \mathbf{x}, \mathbf{y})}{\partial\mathbf{n}(\mathbf{y})}ds(\mathbf{y}) \\
K'\psi(\mathbf{x}) &:= \int_{\Gamma} \psi(\mathbf{y})\frac{\partial\Phi(k, \mathbf{x}, \mathbf{y})}{\partial\mathbf{n}(\mathbf{x})}ds(\mathbf{y}) \\
K'_0\psi(\mathbf{x}) &:= \int_{\Gamma} \psi(\mathbf{y})\frac{\partial\Phi(k_0, \mathbf{x}, \mathbf{y})}{\partial\mathbf{n}(\mathbf{x})}ds(\mathbf{y}) \\
T\psi(\mathbf{x}) &:= \frac{\partial}{\partial\mathbf{n}(\mathbf{x})} \int_{\Gamma} \psi(\mathbf{y})\frac{\partial\Phi(k, \mathbf{x}, \mathbf{y})}{\partial\mathbf{n}(\mathbf{y})}ds(\mathbf{y}) \\
T_0\psi(\mathbf{x}) &:= \frac{\partial}{\partial\mathbf{n}(\mathbf{x})} \int_{\Gamma} \psi(\mathbf{y})\frac{\partial\Phi(k_0, \mathbf{x}, \mathbf{y})}{\partial\mathbf{n}(\mathbf{y})}ds(\mathbf{y})
\end{aligned}$$

We take (2.8)-(2.6) and (2.9)-(2.7) to give us the following integral equations

$$(2 + K_0 - K)u^t + (S - S_0)\frac{\partial u^t}{\partial n} = 2u^i \quad (2.10)$$

$$(2 + K' - K'_0)\frac{\partial u^t}{\partial n} + (T_0 - T)u^t = 2\frac{\partial u^i}{\partial n} \quad (2.11)$$

which we can solve to give numerical approximations for  $u^t$  and  $\partial u/\partial n$  on  $\Gamma$ . Then we can use (2.3) and (2.5) to compute the entire field via a numerical integration over the boundary. Note that we could equally have chosen to solve the boundary integral equations (2.10) and (2.11) for  $u_0$ , since  $u^t = u_0$  on  $\Gamma$ . We see here the benefit of the boundary element method. We have reduced a 2-D problem to a set of 1-D integrals over the boundary. The equivalent integral equation for the acoustic scattering problem in [6] is

$$(I + i\eta S + K')\frac{\partial u^s}{\partial n} = 2i\eta u^i + 2\frac{\partial u^i}{\partial n} \quad (2.12)$$

the main difference being that we seek here to approximate two unknowns. We also note the integral equations we would obtain if we solved for the scattered field,  $u^s$ .

$$\begin{aligned} (2 + K_0 - K)u^t + (S - S_0)\frac{\partial u^t}{\partial n} &= -u^i - K_0u^i + S_0\frac{\partial u^i}{\partial n} \\ (2 + K' - K'_0)\frac{\partial u^t}{\partial n} + (T_0 - T)u^t &= -\frac{\partial u^i}{\partial n} - T_0u^i + K'_0\frac{\partial u^i}{\partial n} \end{aligned} \quad (2.13)$$

The singular term term we referred to earlier is  $T_0u^i$ .

## 2.5 Leading Order Behaviour

One of the major aims in wave scattering is to minimise the computational cost of modelling the scattered wave. For large wavenumber, an efficient method is to examine the leading order behaviour of the field. In the high frequency regime, specifically as  $k \rightarrow \infty$  (equivalent locally to an incident wave upon an infinite plane), the known leading order behaviour in this transmission problem is as follows.

### 2.5.1 Illuminated sides

If a side is illuminated, we expect that the incident wave will produce reflected and transmitted waves as illustrated in figure 2.2.  $u^r$  is the reflected wave,  $u_{tr}$  is the transmitted wave,  $\theta_i$  is the angle of incidence and  $\theta_t$  the angle of transmission.  $z_1$  and  $z_2$  are Cartesian co-ordinates local to the side, and  $n_i$  and  $n_t$  are the refractive indices in  $R^2 \setminus \bar{D}$  and  $D$  respectively.  $u^i, u^r$  and  $u_{tr}$  are described by

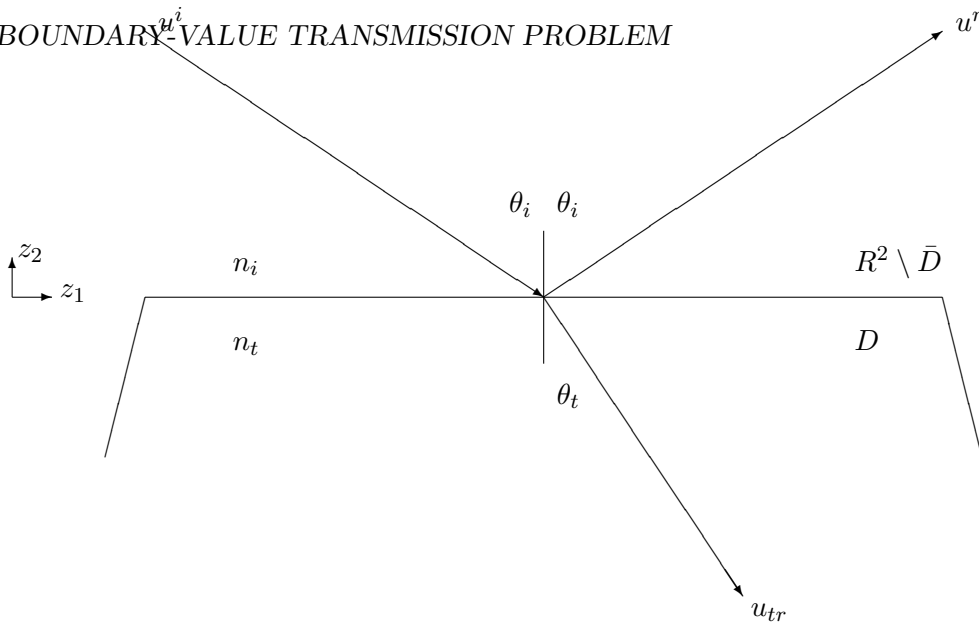


Figure 2.2: Leading order behaviour of the field on an illuminated side

$$\begin{aligned}
 u^i &= e^{ik(z_1 \sin \theta_i - z_2 \cos \theta_i)} \\
 u^r &= R e^{ik(z_1 \sin \theta_i + z_2 \cos \theta_i)} \\
 u_{tr} &= T e^{ik(z_1 \sin \theta_t - z_2 \cos \theta_t)} \\
 \frac{\partial u^i}{\partial \mathbf{n}} &= \frac{\partial u^i}{\partial z_2} = -\cos \theta_i e^{ik(z_1 \sin \theta_i - z_2 \cos \theta_i)} \\
 \frac{\partial u^r}{\partial \mathbf{n}} &= \frac{\partial u^r}{\partial z_2} = R \cos \theta_i e^{ik(z_1 \sin \theta_i - z_2 \cos \theta_i)} \\
 \frac{\partial u_{tr}}{\partial \mathbf{n}} &= \frac{\partial u_{tr}}{\partial z_2} = -T \cos \theta_t e^{ik(z_1 \sin \theta_t - z_2 \cos \theta_t)}
 \end{aligned}$$

Fresnel's law for TE polarised light passing between two media gives the reflection and transmission co-efficients,  $R$  and  $T$ .  $\theta_t$  is obtained from  $\theta_i$  via Snell's law,  $n_i \sin \theta_i = n_t \sin \theta_t$ .

$$R = \frac{n \cos(\theta_i) - n_t \cos(\theta_t)}{n \cos(\theta_i) + n_t \cos(\theta_t)} = \frac{\cos(\theta_i) - \frac{n_t}{n_i} \cos(\theta_t)}{\cos(\theta_i) + \frac{n_t}{n_i} \cos(\theta_t)} = \frac{\cos(\theta_i) - \frac{k_0}{k} \cos(\theta_t)}{\cos(\theta_i) + \frac{k_0}{k} \cos(\theta_t)} \quad (2.14)$$

$$T = \frac{2n_i \cos \theta_i}{n_i \cos \theta_i + n_t \cos \theta_t} = \frac{2 \cos \theta_i}{\cos \theta_i + \frac{n_t}{n_i} \cos \theta_t} = \frac{2 \cos \theta_i}{\cos \theta_i + \frac{k_0}{k} \cos \theta_t} \quad (2.15)$$

Thus on an illuminated side our leading order behaviour is

$$\begin{aligned} u^t \approx u^i + u^r &= (1 + R)u^i \\ \frac{\partial u^t}{\partial n} \approx \frac{\partial u^i}{\partial n} + \frac{\partial u^r}{\partial n} &= (1 - R) \frac{\partial u^i}{\partial n} \\ u_0 &\approx u_{tr} \\ \frac{\partial u_0}{\partial n} &\approx \frac{\partial u_{tr}}{\partial n} \end{aligned} \quad (2.16)$$

where we can gain an explicit representation for  $u_{tr}$  in terms of  $u^i$  and  $T$  if we need to. It takes roughly ten nodes per wavelength (as is the standard in the literature) to give an acceptable approximation to a wave, and as  $k$  increases, the number of nodes required per unit length scales as  $k$ , and is therefore computationally expensive for high frequency scattering. By removing the oscillation of the incident and reflected wave, we have removed the need to model the explicitly known component of the field.

### 2.5.2 Shadow sides

The physical optics approximation on a shadow side is considerably more complicated than for an illuminated side. We first note the principle of total internal reflection. This is the observation that for light passing from one medium to another which is optically less dense (real part of  $n_t <$  real part of  $n_i$ ) 100% of the incident light is reflected when the angle of incidence exceeds an angle known as the critical angle.

Hence on a shadow side there will be two contributions to the field; waves that are transmitted

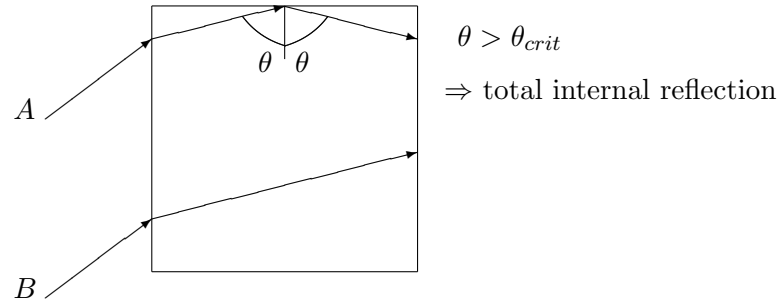


Figure 2.3: Multiple ray contributions at a shadow side

from one side to another that follow a straight line path through  $D$  (marked  $B$  in figure 2.3) and waves that undergo total internal reflection one or more times before arriving at the given side (marked  $A$  in figure 2.3).

We do not attempt here the difficult task of obtaining an analytical expression for the leading order behaviour on a shadow side. Instead, we use the same approximation as [6], that  $u^t \approx 0$  and  $\frac{\partial u^t}{\partial n} \approx 0$ . We remind ourselves that we are only solving for  $u^t$  on  $\Gamma$ , hence we need no approximation for  $u_0$ .

## 2.6 Modified integral equations

Having identified the leading order behaviour, we separate it off and formulate the integral equations.

We let

$$\begin{aligned} u^t &= \varphi_u + \Psi_u \\ \frac{\partial u^t}{\partial n} &= \varphi_{\partial u / \partial n} + \Psi_{\partial u / \partial n} \end{aligned}$$

where

$$\Psi_u = \begin{cases} (1+R)u^i & \text{illuminated sides} \\ 0 & \text{shadow sides} \end{cases}$$

$$\Psi_{\partial u/\partial n} = \begin{cases} (1-R)\frac{\partial u^i}{\partial n} & \text{illuminated sides} \\ 0 & \text{shadow sides} \end{cases}$$

Then (2.10) and (2.11) become

$$(2I + K_0 - K)\varphi_u + (S - S_0)\varphi_{\partial u/\partial n} = (2u^i - \Psi_u) - (K_0 - K)\Phi_u - (S - S_0)\Phi_{\partial u/\partial n} \quad (2.17)$$

$$(T_0 - T)\varphi_u + (2I + K' - K'_0)\varphi_{\partial u/\partial n} = \left(2\frac{\partial u}{\partial n} - \Psi_{\partial u/\partial n}\right) - (T_0 - T)\Phi_u - (K' - K'_0)\Phi_{\partial u/\partial n} \quad (2.18)$$

Thus our new unknowns are  $\varphi_u$  and  $\varphi_{\partial u/\partial n}$ . What do these represent? We can make a comparison with the acoustic scattering problem in [6] to gain a better understanding. As we do here, the leading order behaviour (incident plus reflected field) is subtracted, and (2.12) becomes

$$(I + i\eta S + K')\varphi = 2i\eta u^i + 2\frac{\partial u^i}{\partial n} - (I + i\eta S + K')\Psi$$

where  $1/k\partial u^s/\partial n = \varphi + \Psi$ .  $\Psi = 2\partial u^i/\partial n$  on illuminated sides, and zero on shadow sides.  $\varphi$  represents the field that is diffracted round the corners of the polygon. We note that  $\Psi = \Psi_{\partial u/\partial n}$  when  $R = -1$ . This corresponds to the case when  $k_0 \gg k$ , or when  $\sigma \rightarrow \infty$ , and as we have said, the electric field in  $D$  tends to zero in this case. Then we have the same exterior scattering problem since  $u^t$  must be zero on  $\Gamma$  if it is zero inside, due to the boundary condition that the electric field is continuous across the boundary. So for large values of  $\sigma$ ,  $\varphi_u$  and  $\varphi_{\partial u/\partial n}$  represent the diffracted field on the boundary. If  $\sigma$  is small or zero, then we expect that the incident wave will be primarily transmitted through  $D$ . Then  $u^t$  and  $\partial u^t/\partial n$  are not negligible on shadow sides (see figure 2.5.2). Then  $\varphi_u$  and  $\varphi_{\partial u/\partial n}$  will continue to represent the diffracted field on illuminated sides, while on shadow sides they will represent the diffracted and transmitted fields.

### 3 Parameterisation and the Approximation Space

#### 3.1 Parameterisation

To solve the boundary integral equations, we need to discretise the boundary, and parameterise the variables  $\mathbf{x}$  and  $y$  on the boundary. Schematically we have

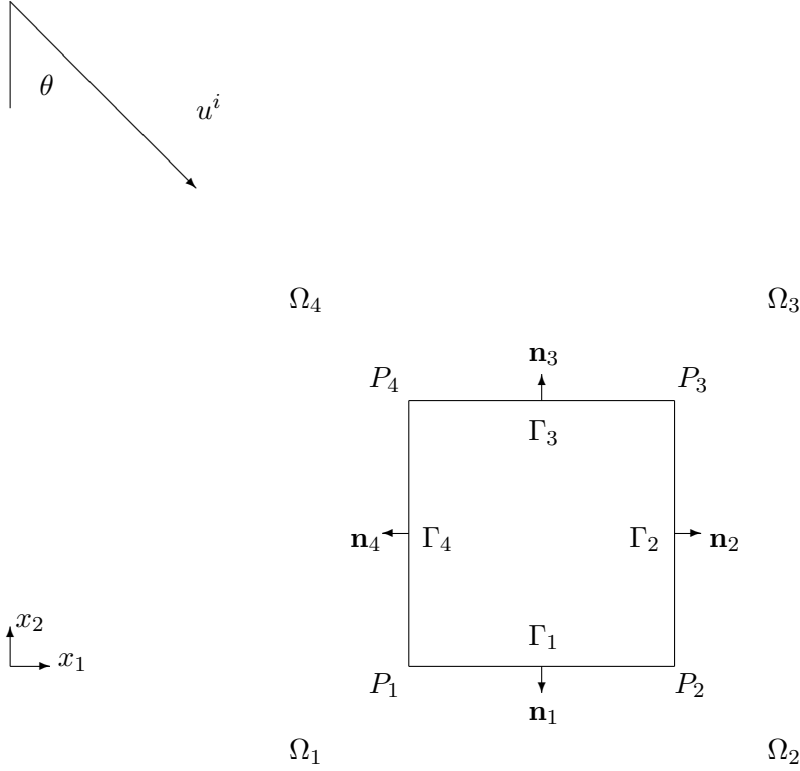


Figure 3.1: Parameterisation

We let  $P_j = (p_j, q_j), j = 1, \dots, n_v$  represent the  $n_v$  vertices of the polygon, with  $P_{n_v+1} = P_1$ .  $\Gamma_j$  is then the line joining  $P_j$  to  $P_{j+1}$ ,  $L_j = |P_{j+1} - P_j|$ , the length of  $\Gamma_j$ , and  $\Omega_j \in (\pi, 2\pi)$  is the external angle at the  $j$ th vertex. We describe the incident wave by  $u^i(\mathbf{x}) = e^{ik\mathbf{x}\cdot\mathbf{d}} = e^{ik(x_1 \sin\theta - x_2 \cos\theta)}$ , where

$\theta$  is measured anti-clockwise from the downwards vertical, and  $d = (\sin \theta, -\cos \theta)$  is the direction of propagation. The unit normal on  $\Gamma_l$  is given by  $\mathbf{n} = (n_1, n_2) = (b_l, -a_l)$ , with

$$\frac{\partial u^i}{\partial \mathbf{n}(\mathbf{x})} = \nabla_{\mathbf{x}} u^i \cdot \mathbf{n}(\mathbf{x}) = \frac{\partial u^i}{\partial x_1} n_1 + \frac{\partial u^i}{\partial x_2} n_2 = (b_l \sin \theta + a_l \cos \theta) u^i$$

We let  $s$  and  $t$  be parametric representations for  $\mathbf{x}$  and  $\mathbf{y}$  respectively, with  $s \in \Gamma_l$  and  $t \in \Gamma_j$ . Then  $s$  and  $t$  are the distance traversed anti-clockwise around the boundary, with  $s = t = 0$  at  $P_1$ . On  $\Gamma_l$  we have

$$\begin{aligned} \mathbf{x}(s) &= P_l + s \left( \frac{P_{l+1} - P_l}{L_l} \right), \quad s \in (0, L_l) \\ &= P_l + \left( s - \sum_{k=1}^{l-1} L_k \right) \left( \frac{P_{l+1} - P_l}{L_l} \right), \quad s \in \Gamma_l \end{aligned}$$

Thus

$$\begin{aligned} x_1(s) &= p_l + \left( s - \sum_{k=1}^{l-1} L_k \right) \left( \frac{p_{l+1} - p_l}{L_l} \right), \quad s \in \Gamma_l \\ x_2(s) &= q_l + \left( s - \sum_{k=1}^{l-1} L_k \right) \left( \frac{q_{l+1} - q_l}{L_l} \right), \quad s \in \Gamma_l \end{aligned}$$

Now we define

$$\begin{aligned}
a_l &:= \frac{p_{l+1} - p_l}{L_l} \\
b_l &:= \frac{q_{l+1} - q_l}{L_l} \\
c_l &:= p_j - a_l \sum_{k=1}^{l-1} L_k \\
d_l &:= q_j - b_l \sum_{k=1}^{l-1} L_k
\end{aligned}$$

which gives us the parameterised variables  $\mathbf{x}(s)$  and  $\mathbf{y}(t)$

$$\begin{aligned}
x_1(s) &= a_l s + c_l, s \in \Gamma_l \\
x_2(s) &= b_l s + d_l \\
y_1(t) &= a_j t + c_j, t \in \Gamma_j \\
y_2(t) &= b_j t + d_j
\end{aligned}$$

### 3.2 The approximation space

We use an identical approximation space to that in [6] and [7]. We recall that the problem there is an exterior acoustic scattering problem, with Dirichlet boundary conditions,  $u = 0$  on  $\Gamma$ . As we have noted (2.12), the initial integral equation formulation has as its unknown,  $\partial u^s / \partial n$  on  $\Gamma$ . After subtraction of the leading order behaviour (incident plus reflected wave), the unknown in the integral equation becomes  $\varphi$ , which is representative of the diffracted field on  $\Gamma$ .  $\varphi$  has the explicit representation

$$\varphi(s) = \frac{i}{2} \left[ e^{iks} v_j^+(s) + e^{-iks} v_j^-(s) \right], s \in \Gamma_j, j = 1, \dots, n_v,$$

$\varphi$  consists of diffracted waves travelling in both directions on the boundary (due to the plane wave  $e^{\pm iks}$  terms), with the amplitude determined by  $v_j^\pm$ . Bounds are given that quantify the behaviour of

$v_j^\pm$  on the sides of the polygon. Essentially, the  $v_j^\pm$  are peaked near the corners (increasingly peaked for more acute corners) and approximately constant away from the corners. This is illustrated in figure 3.2. The peak at  $A$  is due to  $v_j^+ e^{iks}$ , while the peak at  $B$  is due to  $v_{j+1}^- e^{-iks}$ , so that the diffracted wave causes peaked behaviour on the side it is diffracted onto. We do not expect a significant contribution to the peak at  $B$  from  $v_j^+ e^{iks}$ , nor do we expect  $v_{j+1}^- e^{-iks}$  to affect the peak at  $A$ .

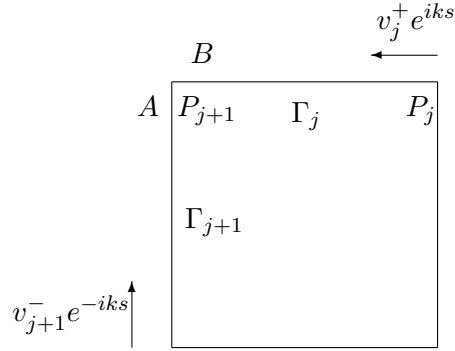


Figure 3.2: Diffracted behaviour at a corner

Thus on  $\Gamma_j$ ,  $v_j^+$  will be peaked near  $P_j$ , and approximately constant away from  $P_j$  and towards  $P_{j+1}$ .  $v_j^-$  will exhibit the opposite, being peaked near  $P_{j+1}$ , and approximately constant as we move towards  $P_j$ . The novelty of the Galerkin scheme in [6] is that the  $v_j^\pm$  are approximated by piecewise polynomials instead of approximating  $\varphi$  directly. The piecewise constants are then multiplied by plane waves travelling in both directions on the boundary to form plane wave basis functions. We follow a similar procedure here, though we do not have analogous results that describe the behaviour of  $\varphi_u$  and  $\varphi_{\partial u/\partial n}$  on  $\Gamma$ . For the ice crystal problem, we expect that  $\varphi_u$  and  $\varphi_{\partial u/\partial n}$  will represent the transmitted plus diffracted fields on shadow sides, and the diffracted field on illuminated sides.

### 3.2.1 The mesh and basis functions

We define the mesh identically to that in [6]. On each side we have two meshes to fit the behaviour of  $v_j^\pm$ . We term *gridx* and *gridy* be the meshes around the boundary consisting of the individual  $v_j^+$  and  $v_j^-$  respectively, so that  $gridx = [v_1^+, \dots, v_{n_v}^+]$  and  $gridy = [v_1^-, \dots, v_{n_v}^-]$ . We let  $n_{gx}$  and  $n_{gy}$  be the number of elements in *gridx* and *gridy*. We denote these by  $\Gamma_j^+$  and  $\Gamma_j^-$ . On  $\Gamma_j^+$  the grading is high (ie the nodes are very close together) at  $P_j$  (where  $v_j^+$  is peaked) and decreases towards  $P_{j+1}$ . On  $\Gamma_j^-$  we have the lowest grading at  $P_j$ , increasing towards  $P_{j+1}$  (where  $v_j^-$  is peaked).

**Definition 3.1** For  $A \geq \lambda, N = 2, 3, \dots$ , the mesh  $\Lambda_{N,A,\lambda,q} = \{y_0, \dots, y_{N+\hat{N}_{A,\lambda,q}}\}$  consists of the points  $y_i = \lambda \left(\frac{i}{N}\right)^q, i = 0, \dots, N$ , and the points  $y_{N+j} = \lambda \left(\frac{A}{\lambda}\right)^{\frac{j}{\hat{N}_{A,\lambda,q}}}, j = 1, \dots, \hat{N}_{A,\lambda,q}$  where  $\hat{N}_{A,\lambda,q} = \lceil N^* \rceil$  is the smallest integer greater than or equal to  $N^*$ , with  $N^* = -\frac{\log(\frac{A}{\lambda})}{q \log(1 - \frac{1}{N})}$ . For  $j = 1, \dots, n$  we define  $\alpha_j := 1 - \frac{\pi}{\omega_j}$  and  $q_j := \frac{(2\nu+3)}{(1-2\alpha_j)}$ .

Then the meshes  $\Gamma_j^+$  and  $\Gamma_j^-$  are

$$\begin{aligned}\Gamma_j^+ &:= P_j + \Lambda_{N,L_j,\lambda,q_j} \\ \Gamma_j^- &:= P_{j+1} - \Lambda_{N,L_j,\lambda,q_{j+1}}\end{aligned}$$

For  $s \in [0, L]$  we define

$$\begin{aligned}V_{\Gamma_j^+,\nu} &:= \left\{ \sigma e^{iks} : \sigma \in C \right\} \\ V_{\Gamma_j^-,\nu} &:= \left\{ \sigma e^{-iks} : \sigma \in C \right\}\end{aligned}$$

and the approximation space,  $V_{\Gamma,\nu}$ , is the linear span of

$$\bigcup_{j=1,\dots,n} \left\{ V_{\Gamma_j^+,\nu} \cup V_{\Gamma_j^-,\nu} \right\}$$

The basis functions,  $\rho_j(t)$  are defined by

$$\rho_j(t) := \frac{e^{ik\sigma_j t} \xi_{[y_j, y_{j+1}]}}{\sqrt{(y_{j+1} - y_j)}}$$

where  $\xi_{[y_j, y_{j+1}]}$  is the characteristic function for the interval  $[y_j, y_{j+1}]$ .  $\xi_{[y_j, y_{j+1}]} = 1$  if  $s \in [y_j, y_{j+1}]$ , zero otherwise.

There are a few points to note here.  $\nu$  is the degree of polynomial we use in our basis function. Here we use piecewise constants so  $\nu = 0$ . On  $\Gamma_j^\pm$  we have a composite mesh. The high grading occurs on the interval  $[0, \lambda]$  with  $N$  mesh points separated by a polynomial grading. On the interval  $[\lambda, A]$  there is a geometric grading for  $\hat{N}_{A, \lambda, q}$  mesh points. The choice of  $N^*$  ensures that the polynomial and geometric meshes exhibit a smooth transition. We take  $A = L_j$  so that the mesh covers every side in both directions. We also note that the mesh grading is determined by  $\alpha_j$ , which in turn is determined by the corner angle  $\omega_j$ . The dependence is such that the approximation error in  $\varphi$  in [6] is equidistributed across the intervals of the mesh.

Lastly we note that for the basis function  $\rho_j$ ,  $\sigma_j = +1$  if  $\rho_j$  is on *gridx* and  $-1$  if it is on *gridy*.

## 4 The Galerkin Method

We recall the integral equations (2.17) and (2.18)

$$\begin{aligned} (2I + K_0 - K)\varphi_u + (S - S_0)\varphi_{\partial u/\partial n} &= (2u^i - \Psi_u) - (K_0 - K)\Phi_u - (S - S_0)\Phi_{\partial u/\partial n} \\ (T_0 - T)\varphi_u + (2I + K' - K'_0)\varphi_{\partial u/\partial n} &= 2\frac{\partial u}{\partial n} - \Psi_{\partial u/\partial n} - (T_0 - T)\Phi_u - (K' - K'_0)\Phi_{\partial u/\partial n} \end{aligned}$$

We approximate  $\varphi_u$  and  $\varphi_{\partial u/\partial n}$  as a linear combination of the basis functions,  $\rho_j$

$$\varphi_u = \sum_{j=1}^{n_g} u_j \rho_j(s), 0 \leq s \leq L \quad (4.1)$$

$$\varphi_{\partial u / \partial n} = \sum_{j=1}^{n_g} v_j \rho_j(s), 0 \leq s \leq L \quad (4.2)$$

where  $n_g = n_{gx} + n_{gy}$ , the total number of elements in our approximation space, and  $u_j$  and  $v_j$  are the unknowns that we seek to determine. We then have

$$(2I + K_0 - K) \sum_{j=1}^{n_g} u_j \rho_j(s) + (S - S_0) \sum_{j=1}^{n_g} v_j \rho_j(s) = (2u^i - \Psi_u) - (K_0 - K)\Phi_u - (S - S_0)\Phi_{\partial u / \partial n} = F$$

$$(T_0 - T) \sum_{j=1}^{n_g} u_j \rho_j(s) + (2 + K' - K'_0) \sum_{j=1}^{n_g} v_j \rho_j(s) = 2 \frac{\partial u}{\partial \mathbf{n}} - \Psi_{\partial u / \partial n} - (T_0 - T)\Phi_u - (K' - K'_0)\Phi_{\partial u / \partial n} = G$$

where we use  $F$  and  $G$  for clarity. Defining the inner product on  $L^2(0, L)$  by  $(\tau_1, \tau_2) = \int_0^L \tau_1(t) \bar{\tau}_2(t) dt$ , we multiply by a second basis function,  $\rho_m(s)$ , and apply the inner product to obtain the following linear system

$$\sum_{j=1}^{n_g} [u_j [(2\rho_j, \rho_m) + ((K_0 - K)\rho_j, \rho_m)] + v_j [(S - S_0)\rho_j, \rho_m]] = \sum_{j=1}^{n_g} [u_j A_{jm} + v_j B_{jm}] = (F, \rho_m)$$

$$\sum_{j=1}^{n_g} [u_j [(T_0 - T)\rho_j, \rho_m]] + v_j [(2\rho_j, \rho_m) + ((K' - K'_0)\rho_j, \rho_m)] = \sum_{j=1}^{n_g} [u_j C_{jm} + v_j D_{jm}] = (G, \rho_m)$$

This is re-written as a matrix equation

$$\begin{bmatrix} A_{11} & A_{12} & \cdots & B_{11} & B_{12} & \cdots \\ A_{21} & \ddots & \ddots & B_{21} & \ddots & \ddots \\ \vdots & \ddots & \ddots & \vdots & \ddots & \ddots \\ C_{11} & C_{12} & \cdots & D_{11} & D_{12} & \cdots \\ C_{21} & \ddots & \ddots & D_{21} & \ddots & \ddots \\ \vdots & \ddots & \ddots & \vdots & \ddots & \ddots \end{bmatrix} \begin{bmatrix} u_1 \\ u_2 \\ \vdots \\ v_1 \\ v_2 \\ \vdots \end{bmatrix} = \begin{bmatrix} (F, \rho_1) \\ (F, \rho_2) \\ \vdots \\ (G, \rho_1) \\ (G, \rho_2) \\ \vdots \end{bmatrix}$$

In the following sections we describe the evaluation of the integrals in the matrix and right hand vector. Once we have these, we solve the matrix equation (using the inbuilt solve function in Matlab) to find the co-efficients  $u_i$  and  $v_i$ , which completes our approximation to  $\varphi_u$  and  $\varphi_{\partial u/\partial n}$  via (4.1) and (4.2). Then we compute the field everywhere using (2.3) and (2.5), but substituting  $u^t = \varphi_u + \Psi_u$  and  $\partial u^t/\partial n = \varphi_{\partial u/\partial n} + \Psi_{\partial u/\partial n}$ . Then

$$\begin{aligned} -u_0(\mathbf{x}) &= \int_{\Gamma} \left[ (\varphi_u + \Psi_u) \frac{\partial \Phi_0(\mathbf{x}, \mathbf{y})}{\partial \mathbf{n}(\mathbf{y})} - (\varphi_{\partial u/\partial n} + \Psi_{\partial u/\partial n}) \Phi(k_0, \mathbf{x}, \mathbf{y}) \right] ds(\mathbf{y}), \quad \mathbf{x} \in D \\ u^t(\mathbf{x}) &= \int_{\Gamma} \left[ (\varphi_u + \Psi_u) \frac{\partial \Phi(k, \mathbf{x}, \mathbf{y})}{\partial \mathbf{n}(\mathbf{y})} - (\varphi_{\partial u/\partial n} + \Psi_{\partial u/\partial n}) \Phi(k, \mathbf{x}, \mathbf{y}) \right] ds(\mathbf{y}) + u^i(\mathbf{x}), \quad \mathbf{x} \in R^2 \setminus \bar{D} \end{aligned}$$

#### 4.1 Left Hand Side

We have five integrals to determine for the left hand side of the matrix equation.

$$L_1 = (2\rho_j, \rho_m)$$

$$L_2 = ((K_0 - K)\rho_j, \rho_m)$$

$$L_3 = ((K' - K_0)\rho_j, \rho_m)$$

$$L_4 = ((S - S_0)\rho_j, \rho_m)$$

$$L_5 = ((T_0 - T)\rho_j, \rho_m)$$

4.1.1  $L_1$ 

$$\begin{aligned}
(2\rho_j, \rho_m) &= 2 \int_0^L \rho_j(s) \bar{\rho}_m(s) ds \\
&= 2 \int_{\text{supp}(\rho_j) \cap \text{supp}(\rho_m)} \frac{e^{iks(\sigma_j - \sigma_m)}}{\sqrt{(y_{m+1} - y_m)} \sqrt{(y_{j+1} - y_j)}} ds
\end{aligned} \tag{4.3}$$

The basis functions are defined only on their intervals, so  $L_1$  is non-zero where the basis functions overlap. Denoting  $rh$  and  $lh$  to be the ends of the overlap,

$$L_1 = \begin{cases} \frac{2(e^{ik(\sigma_j - \sigma_m)rh} - e^{ik(\sigma_j - \sigma_m)lh})}{ik(\sigma_j - \sigma_m)\sqrt{(y_{j+1} - y_j)(y_{m+1} - y_m)}} & \sigma_j \neq \sigma_m \\ \frac{2(rh - lh)}{\sqrt{(y_{j+1} - y_j)(y_{m+1} - y_m)}} & \sigma_j = \sigma_m \end{cases}$$

4.1.2  $L_2$  and  $L_3$ 

We recall that

$$K\psi(\mathbf{x}) = 2 \int_{\Gamma} \frac{\partial \Phi(k, \mathbf{x}, \mathbf{y})}{\partial \mathbf{n}(\mathbf{y})} \psi(\mathbf{y}) ds(\mathbf{y})$$

where

$$\frac{\partial \Phi(k, \mathbf{x}, \mathbf{y})}{\partial \mathbf{n}(\mathbf{y})} = \nabla_{\mathbf{y}} \Phi(k, \mathbf{x}, \mathbf{y}) \cdot \mathbf{n}(\mathbf{y}) = \frac{\partial \Phi(k, \mathbf{x}, \mathbf{y})}{\partial y_1} n_1 + \frac{\partial \Phi(k, \mathbf{x}, \mathbf{y})}{\partial y_2} n_2$$

$$\Phi(k, \mathbf{x}, \mathbf{y}) = \frac{i}{4} H_0^{(1)}(kR), R = |\mathbf{x} - \mathbf{y}| = [(x_1 - y_1)^2 + (x_2 - y_2)^2]^{\frac{1}{2}}$$

We have that  $\frac{d}{dz} H_n^{(1)}(z) = \frac{n H_n^{(1)}(z)}{z} - H_{n+1}^{(1)}(z)$ . Hence

$$K\psi(\mathbf{x}) = 2 \int_{\Gamma} \frac{ik H_1^{(1)}(kR)}{4 R} [(x_1 - y_1)n_1(\mathbf{y}) + (x_2 - y_2)n_2(\mathbf{y})] \psi(\mathbf{y}) ds(\mathbf{y})$$

For the adjoint of  $K, K'$ , we replace  $\frac{\partial \Phi(k, \mathbf{x}, \mathbf{y})}{\partial \mathbf{n}(\mathbf{y})}$  with  $\frac{\partial \Phi(k, \mathbf{x}, \mathbf{y})}{\partial \mathbf{n}(\mathbf{x})}$ , giving

$$K'\psi(\mathbf{x}) = 2 \int_{\Gamma} \frac{-ik}{4} \frac{H_1^{(1)}(kR)}{R} [(x_1 - y_1)n_1(\mathbf{x}) + (x_2 - y_2)n_2(\mathbf{x})] \psi(\mathbf{y}) ds(\mathbf{y})$$

Now we parameterise using  $s$  and  $t$ ,  $s \in \Gamma_l$  and  $t \in \Gamma_j$  (see section 3.1), to obtain the integrals in parameterised form

$$\begin{aligned} K\psi(s) &= 2 \int_{\Gamma} k(s, t)\psi(t) dt \\ K'\psi(s) &= 2 \int_{\Gamma} k'(s, t)\psi(t) dt \end{aligned}$$

where

$$\begin{aligned} k(s, t) &= \frac{ik}{4} \frac{H_1^{(1)}(kR)}{R} [(a_l b_j - b_l a_j)s + (c_l - c_j)b_j - (d_l - d_j)a_j] \\ k'(s, t) &= \frac{-ik}{4} \frac{H_1^{(1)}(kR)}{R} [(a_l b_j - b_l a_j)t + (c_l - c_j)b_l - (d_l - d_j)a_l] \end{aligned}$$

Then

$$\begin{aligned} (k_0 - k)(s, t) &= \frac{i}{4} \frac{(k_0 H_1^{(1)}(k_0 R) - k H_1^{(1)}(kR))}{R} [(a_l b_j - b_l a_j)s + (c_l - c_j)b_j - (d_l - d_j)a_j] \\ (k' - k'_0)(s, t) &= \frac{-i}{4} \frac{(k H_1^{(1)}(kR) - k_0 H_1^{(1)}(k_0 R))}{R} [(a_l b_j - b_l a_j)t + (c_l - c_j)b_l - (d_l - d_j)a_l] \end{aligned}$$

Thus,

$$\begin{aligned} L_2 = ((K_0 - K)\rho_j, \rho_m) &= \int_{\text{supp}(\rho_m)} \left[ \int_{\text{supp}(\rho_j)} [k_0(s, t) - k(s, t)] \rho_j(t) dt \right] \rho_m(s) ds \\ L_2 &= 2 \int_{y_m}^{y_{m+1}} \int_{y_j}^{y_{j+1}} \frac{(k_0 - k)(s, t) e^{ik(\sigma_j t - \sigma_m s)}}{\sqrt{(y_{m+1} - y_m)(y_{j+1} - y_j)}} dt ds \end{aligned}$$

and

$$L_3 = 2 \int_{y_m}^{y_{m+1}} \int_{y_j}^{y_{j+1}} \frac{(k' - k'_0)(s, t) e^{ik(\sigma_j t - \sigma_m s)}}{\sqrt{(y_{m+1} - y_m)(y_{j+1} - y_j)}} dt ds$$

We evaluate these, and all the integrals that follow that are not analytic, numerically using Gaussian quadrature. Further details are given in section 4. We observe that for  $l = j$ , when  $s$  and  $t$  lie on the same side of the polygon  $(k_0 - k)(s, t) = (k' - k'_0)(s, t) = 0$ , and therefore  $L_2$  and  $L_3$  are zero.

#### 4.1.3 $L_4$

$S\psi(\mathbf{x}) = 2 \int_{\Gamma} \Phi(k, \mathbf{x}, \mathbf{y}) \psi(\mathbf{y}) ds(\mathbf{y})$ , and analogous to the evaluation of  $L_3$  and  $L_4$ , we have the parameterised kernel  $(s - s_0)(s, t) = \frac{i}{4}(H_0^{(1)}(kR) - H_0^{(1)}(k_0R))$ . For  $l \neq j$ ,

$$L_4 = 2 \int_{y_m}^{y_{m+1}} \int_{y_j}^{y_{j+1}} \frac{(s - s_0)(s, t) e^{ik(\sigma_j t - \sigma_m s)}}{\sqrt{(y_{m+1} - y_m)(y_{j+1} - y_j)}} dt ds$$

For  $l = j$ , we can evaluate some of the integral analytically. We note that  $R = |s - t|$ , and use the following integral representation for the Hankel function [9, 12.31]

$$H_0^{(1)}(s) = \frac{-2i}{\pi} \int_0^\infty \frac{e^{(i-r)s}}{r^{\frac{1}{2}}(r - 2i)^{\frac{1}{2}}} dr, s > 0$$

$$L_4 = 2 \int_{y_m}^{y_{m+1}} \int_{y_j}^{y_{j+1}} \frac{i}{4} \left[ \frac{-2i}{\pi} \int_0^\infty \frac{e^{(i-r)k|s-t|} - e^{(i-r)k_0|s-t|}}{r^{\frac{1}{2}}(r - 2i)^{\frac{1}{2}}} \right] \frac{e^{ik(\sigma_j t - \sigma_m s)}}{\sqrt{(y_{m+1} - y_m)(y_{j+1} - y_j)}} dt ds$$

We re-arrange the order of integration to obtain

$$L_4 = \frac{1}{\pi \sqrt{(y_{m+1} - y_m)(y_{j+1} - y_j)}} \int_0^\infty \frac{I(r)}{r^{\frac{1}{2}}(r - 2i)^{\frac{1}{2}}} dr \quad (4.4)$$

where

$$I(r) = \int_{y_m}^{y_{m+1}} \int_{y_j}^{y_{j+1}} e^{(i-r)k|s-t|+ik(\sigma_j t - \sigma_m s)} - e^{(i-r)k_0|s-t|+ik(\sigma_j t - \sigma_m s)} dt ds$$

We evaluate  $I(r)$  analytically as follows. If  $y_{j+1} < y_m, s > t, |s - t| = (s - t)$ ,

$$\begin{aligned} I(r) &= \left[ \frac{e^{((i-r)k-ik\sigma_m)a} - e^{((i-r)k-ik\sigma_m)b}}{(i-r)k - ik\sigma_m} \right] \left[ \frac{e^{((r-i)k+ik\sigma_j)d} - e^{((r-i)k+ik\sigma_j)c}}{(r-i)k + ik\sigma_j} \right] \\ &- \left[ \frac{e^{((i-r)k_0-ik\sigma_m)b} - e^{((i-r)k_0-ik\sigma_m)a}}{(i-r)k_0 - ik\sigma_m} \right] \left[ \frac{e^{((r-i)k_0+ik\sigma_j)d} - e^{((r-i)k_0+ik\sigma_j)c}}{(r-i)k_0 + ik\sigma_j} \right] \end{aligned} \quad (4.5)$$

If  $y_{m+1} < y_j, t > s, |s - t| = (t - s)$ ,

$$\begin{aligned} I(r) &= \left[ \frac{e^{((r-i)k-ik\sigma_m)b} - e^{((r-i)k-ik\sigma_m)a}}{(r-i)k - ik\sigma_m} \right] \left[ \frac{e^{((i-r)k+ik\sigma_j)d} - e^{((i-r)k+ik\sigma_j)c}}{(i-r)k + ik\sigma_j} \right] \\ &- \left[ \frac{e^{((r-i)k_0-ik\sigma_m)b} - e^{((r-i)k_0-ik\sigma_m)a}}{(r-i)k_0 - ik\sigma_m} \right] \left[ \frac{e^{((i-r)k_0+ik\sigma_j)d} - e^{((i-r)k_0+ik\sigma_j)c}}{(i-r)k_0 + ik\sigma_j} \right] \end{aligned} \quad (4.6)$$

where  $a = y_m, b = y_{m+1}, c = y_j, d = y_{j+1}$ . If the intervals overlap, then we split  $I(r)$  into three separate double integrals. For example, consider the overlapping basis functions illustrated below

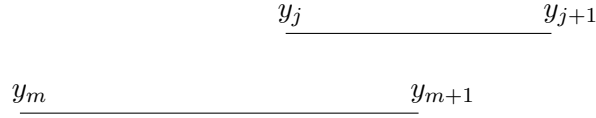


Figure 4.1: Overlapping basis functions

We can consider  $I(r)$  to be the sum of (4.6) with  $a = y_m, b = y_j, c = y_j, d = y_{j+1}$ , plus (4.6) with  $a = y_j, b = y_{m+1}, c = y_{m+1}, d = y_{j+1}$ , plus the double integral (where  $a = y_j, b = y_{m+1}$ )

$$\begin{aligned}
& \int_a^b \int_a^b e^{(i-r)k|s-t|+ik(\sigma_j t-\sigma_m s)} - e^{(i-r)k_0|s-t|+ik(\sigma_j t-\sigma_m s)} dt ds \\
&= \int_a^b \int_a^s e^{(i-r)k(s-t)+ik(\sigma_j t-\sigma_m s)} - e^{(i-r)k_0(s-t)+ik(\sigma_j t-\sigma_m s)} dt ds \\
&+ \int_a^b \int_s^b e^{(i-r)k(t-s)+ik(\sigma_j t-\sigma_m s)} - e^{(i-r)k_0(t-s)+ik(\sigma_j t-\sigma_m s)} dt ds \\
&+ \frac{1}{(r-i)k+ik\sigma_j} \left[ \frac{e^{(ik(\sigma_j-\sigma_m))b} - e^{(ik(\sigma_j-\sigma_m))a}}{ik(\sigma_j-\sigma_m)} - \frac{e^{(r-i)k(a-b)+ik(\sigma_j b-\sigma_m a)} - e^{ik(\sigma_j-\sigma_m)a}}{(i-r)k-ik\sigma_m} \right] \\
&- \frac{1}{(r-i)k_0+ik\sigma_j} \left[ \frac{e^{(ik(\sigma_j-\sigma_m))b} - e^{(ik(\sigma_j-\sigma_m))a}}{ik(\sigma_j-\sigma_m)} - \frac{e^{(r-i)k_0(a-b)+ik(\sigma_j b-\sigma_m a)} - e^{ik(\sigma_j-\sigma_m)a}}{(i-r)k_0-ik\sigma_m} \right] \\
&- \frac{1}{(i-r)k+ik\sigma_j} \left[ \frac{e^{(ik(\sigma_j-\sigma_m))b} - e^{(ik(\sigma_j-\sigma_m))a}}{ik(\sigma_j-\sigma_m)} - \frac{e^{ik(\sigma_j-\sigma_m)b} - e^{(r-i)k(a-b)+ik(\sigma_j a-\sigma_m b)}}{(r-i)k-ik\sigma_m} \right] \\
&+ \frac{1}{(i-r)k_0+ik\sigma_j} \left[ \frac{e^{(ik(\sigma_j-\sigma_m))b} - e^{(ik(\sigma_j-\sigma_m))a}}{ik(\sigma_j-\sigma_m)} - \frac{e^{ik(\sigma_j-\sigma_m)b} - e^{(r-i)k_0(a-b)+ik(\sigma_j a-\sigma_m b)}}{(r-i)k_0-ik\sigma_m} \right]
\end{aligned}$$

Returning to (4.4), we now know  $I(r)$ , but the integral is singular at  $r = 0$ . We remedy this by making the substitution  $r = \frac{s^2}{1-s^2}$ , which removes the singularity.

#### 4.1.4 $L_5$

$$\begin{aligned}
T\psi(\mathbf{x}) &= 2 \frac{\partial}{\partial \mathbf{n}(\mathbf{x})} \int_{\Gamma} \frac{\partial \Phi(k, \mathbf{x}, \mathbf{y})}{\partial \mathbf{n}(\mathbf{y})} \psi(\mathbf{y}) ds(\mathbf{y}) \\
&= \frac{\partial}{\partial \mathbf{n}(\mathbf{x})} [K\psi(\mathbf{x})] \\
&= 2 \int_{\Gamma} \left[ \frac{\partial}{\partial x_1} \left( \frac{\partial \Phi(k, \mathbf{x}, \mathbf{y})}{\partial \mathbf{n}(\mathbf{y})} \right) n_1(\mathbf{x}) + \frac{\partial}{\partial x_2} \left( \frac{\partial \Phi(k, \mathbf{x}, \mathbf{y})}{\partial \mathbf{n}(\mathbf{y})} \right) n_2(\mathbf{x}) \right] \psi(\mathbf{y}) ds(\mathbf{y})
\end{aligned}$$

Recalling  $\frac{\partial \Phi(k, \mathbf{x}, \mathbf{y})}{\partial \mathbf{n}(\mathbf{y})}$  and the derivative of  $H_n^{(1)}$ ,

$$\frac{\partial}{\partial x_1} \frac{\partial \Phi(k, \mathbf{x}, \mathbf{y})}{\partial \mathbf{n}(\mathbf{y})} = \frac{\partial}{\partial x_1} \left[ \frac{ik}{4} H_1^{(1)}(kR) \cdot R^{-1} \cdot [(x_1 - y_1)n_1(\mathbf{y}) + (x_2 - y_2)n_2(\mathbf{y})] \right]$$

$$= \frac{i}{4} \begin{bmatrix} \left( \frac{H_1^{(1)}(kR)}{kR} - H_1^{(2)}(kR) \right) \frac{k^2(x_1 - y_1)}{R} & \frac{1}{R} & [(x_1 - y_1)n_1(\mathbf{y}) + (x_2 - y_2)n_2(\mathbf{y})] \\ +kH_1^{(1)}(kR) & \frac{-(x_1 - y_1)}{R^3} & [(x_1 - y_1)n_1(\mathbf{y}) + (x_2 - y_2)n_2(\mathbf{y})] \\ +kH_1^{(1)}(kR) & \frac{-(x_1 - y_1)}{R^3} & n_1(\mathbf{y}) \end{bmatrix}$$

$\frac{\partial}{\partial x_2} \frac{\partial \Phi(k, \mathbf{x}, \mathbf{y})}{\partial \mathbf{n}(\mathbf{y})}$  follows as above, replacing  $(x_1 - y_1)$  by  $(x_2 - y_2)$ , and  $n_1(\mathbf{y})$  by  $n_2(\mathbf{y})$ . After parameterising  $\mathbf{x}$  and  $\mathbf{y}$ , we have for  $l \neq j$

$$L_5 = 2 \int_{y_m}^{y_{m+1}} \int_{y_j}^{y_{j+1}} \frac{(t_0 - t)(s, t) e^{ik(\sigma_j t - \sigma_m s)}}{\sqrt{(y_{m+1} - y_m)(y_{j+1} - y_j)}} dt ds$$

where

$$\begin{aligned} (t_0 - t)(s, t) &= [(a_l b_j - b_l a_j)s + (c_l - c_j)b_j - (d_l - d_j)a_j] [(a_l b_j - b_l a_j)t + (c_l - c_j)b_l - (d_l - d_j)a_l] \\ &\times \left[ \frac{k_0^2}{R} \left( \frac{H_1^{(1)}(k_0 R)}{k_0 R} - H_2^{(1)}(k_0 R) \right) - \frac{k^2}{R} \left( \frac{H_1^{(1)}(kR)}{kR} - H_2^{(1)}(kR) \right) + \frac{kH_1^{(1)}(kR)}{R^3} - \frac{k_0 H_1^{(1)}(k_0 R)}{R^3} \right] \\ &+ \frac{(b_j b_l + a_j a_l)}{R} \left( k_0 H_1^{(1)}(k_0 R) - k H_1^{(1)}(kR) \right) \end{aligned}$$

For  $l = j$ , the kernel reduces to

$$(t_0 - t)(s, t) = (b_j^2 + a_j^2) \frac{(k_0 H_1^{(1)}(k_0 R) - k H_1^{(1)}(kR))}{R}$$

When  $R = 0$  (the intervals coincide or share a common end), the Hankel function, and therefore the kernel is undefined. We use the asymptotic behaviour as  $z \rightarrow 0$  of the bessel functions  $J_\nu(z)$  and  $Y_\nu(z)$  [1, chapter 9]

$$\begin{aligned}
H_1^{(1)}(z) &= J_1(z) + iY_1(z) \\
&\approx \frac{z}{2\Gamma(2)} - \frac{2i\Gamma(1)}{\pi z}, \quad \text{as } z \rightarrow 0 \\
&= \frac{z}{2} - \frac{2i}{\pi z}
\end{aligned}$$

Therefore the kernel becomes

$$\begin{aligned}
(t_0 - t)(s, t) &= (b_j^2 + a_j^2) \frac{(k_0(\frac{k_0 R}{2} - \frac{2i}{\pi k_0 R}) - k(\frac{k R}{2} - \frac{2i}{\pi k R}))}{R} \\
&= (b_j^2 + a_j^2) \left[ \frac{1}{2}(k_0^2 - k^2) - \frac{2i}{\pi R^2} + \frac{2i}{\pi R^2} \right] \\
&= (b_j^2 + a_j^2) \frac{1}{2}(k_0^2 - k^2)
\end{aligned} \tag{4.7}$$

We recall (2.13), and see that the  $T_0 u^i$  term will be singular, since we have no cancellation of the singular term, and our choice to solve for the total, not scattered, field is justified.

## 4.2 Right Hand Side

We have six integrals to determine for the right hand side.

$$\begin{aligned}
R_1 &= (2u^i - 2\Psi_u, \rho_m) \\
R_2 &= (2\frac{\partial u^i}{\partial n} - 2\Psi_{\partial u/\partial n}, \rho_m) \\
R_3 &= ((K_0 - K)\Psi_u, \rho_m) \\
R_4 &= ((K' - K'_0)\Psi_{\partial u/\partial n}, \rho_m) \\
R_5 &= ((S - S_0)\Psi_{\partial u/\partial n}, \rho_m) \\
R_6 &= ((T_0 - T)\Psi_u, \rho_m)
\end{aligned}$$

4.2.1  $R_1$  and  $R_2$ 

$$(2u^i - 2\Psi_u, \rho_m) = \int_{y_m}^{y_{m+1}} \frac{(2u^i - 2\Psi_u)e^{-ik\sigma_m s}}{\sqrt{(y_{m+1} - y_m)}} ds$$

On shadow sides,  $\Psi_u = 0$ , so we have

$$R_1 = \int_{y_m}^{y_{m+1}} \frac{2e^{ik[(a_1 s + c_l)\sin\theta - (b_1 s + d_l)\cos\theta] - ik\sigma_m s}}{\sqrt{(y_{m+1} - y_m)}} ds \quad (4.8)$$

On illuminated sides,  $\Psi_u = (1 + R)u^i$ ,  $(2u^i - 2\Psi_u) = -2Ru^i$ , so we have (4.8) multiplied by a factor of  $-R$ . We also have  $\Psi_{\partial u/\partial n} = 0$  on shadow sides, so

$$R_2 = \int_{y_m}^{y_{m+1}} \frac{2[b_l \sin\theta + a_l \cos\theta] e^{ik[(a_1 s + c_l)\sin\theta - (b_1 s + d_l)\cos\theta] - ik\sigma_m s}}{\sqrt{(y_{m+1} - y_m)}} ds \quad (4.9)$$

On illuminated sides,  $\Psi_u = (1 - R)\partial u^i/\partial n$ ,  $(2\partial u^i/\partial n - 2\Psi_{\partial u/\partial n}) = 2R\partial u^i/\partial n$ , and we have (4.9) multiplied by  $R$ . Thus

$$R_1 = \begin{cases} \frac{2e^{ik(c_l \sin\theta - d_l \cos\theta)}}{ik(a_1 \sin\theta - b_1 \cos\theta - \sigma_m)\sqrt{(y_{m+1} - y_m)}} (e^{ik(a_1 \sin\theta - b_1 \cos\theta - \sigma_m)y_{m+1}} - e^{ik(a_1 \sin\theta - b_1 \cos\theta - \sigma_m)y_m}) & \text{shadow side} \\ \frac{-2R_l e^{ik(c_l \sin\theta - d_l \cos\theta)}}{ik(a_1 \sin\theta - b_1 \cos\theta - \sigma_m)\sqrt{(y_{m+1} - y_m)}} (e^{ik(a_1 \sin\theta - b_1 \cos\theta - \sigma_m)y_{m+1}} - e^{ik(a_1 \sin\theta - b_1 \cos\theta - \sigma_m)y_m}) & \text{illuminated side} \end{cases}$$

Likewise

$$R_2 = \begin{cases} \frac{2(b_l \sin\theta + a_l \cos\theta)e^{ik(c_l \sin\theta - d_l \cos\theta)}}{ik(a_1 \sin\theta - b_1 \cos\theta - \sigma_m)\sqrt{(y_{m+1} - y_m)}} (e^{ik(a_1 \sin\theta - b_1 \cos\theta - \sigma_m)y_{m+1}} - e^{ik(a_1 \sin\theta - b_1 \cos\theta - \sigma_m)y_m}) & \text{shadow side} \\ \frac{2R_l(b_l \sin\theta + a_l \cos\theta)e^{ik(c_l \sin\theta - d_l \cos\theta)}}{ik(a_1 \sin\theta - b_1 \cos\theta - \sigma_m)\sqrt{(y_{m+1} - y_m)}} (e^{ik(a_1 \sin\theta - b_1 \cos\theta - \sigma_m)y_{m+1}} - e^{ik(a_1 \sin\theta - b_1 \cos\theta - \sigma_m)y_m}) & \text{illuminated side} \end{cases}$$

4.2.2  $R_3, R_4, R_5, R_6$ 

$$\begin{aligned} R_3 &= ((K_0 - K)\Psi_u, \rho_m) \\ &= 2 \int_{y_m}^{y_{m+1}} \int_{\sum_{j=1}^{n_s} L_j}^L \frac{(k_0 - k)(s, t)\Psi(t)dt e^{-ik\sigma_m s}}{\sqrt{(y_{m+1} - y_m)}} ds \end{aligned}$$

We change the order of integration and split the integral over the illuminated sides to a sum of the integrals over each illuminated side, denoting the reflection co-efficient on  $\Gamma_k$  by  $R_k$

$$\begin{aligned} R_3 &= 2 \sum_{j=n_s+1}^n \int_{\sum_{p=1}^{j-1} L_p}^{\sum_{p=1}^j L_p} \left[ \int_{y_m}^{y_{m+1}} \frac{(k_0 - k)(s, t) \Psi(t) ds e^{-ik\sigma_m s}}{\sqrt{(y_{m+1} - y_m)}} \right] \Psi(t) dt \\ &= 2 \sum_{j=n_s+1}^n (1 + R_k) e^{ik(c_j \sin\theta - d_j \cos\theta)} \int_{\sum_{p=1}^{j-1} L_p}^{\sum_{p=1}^j L_p} \int_{y_m}^{y_{m+1}} \frac{(k_0 - k)(s, t) e^{ik[(a_j \sin\theta - b_j \cos\theta)t - \sigma_m s]}}{\sqrt{(y_{m+1} - y_m)}} ds dt \end{aligned}$$

Similarly

$$\begin{aligned} R_4 &= 2 \sum_{j=n_s+1}^n (1 - R_k) [b_j \cos\theta + a_j \sin\theta] e^{ik(c_j \sin\theta - d_j \cos\theta)} \int_{\sum_{p=1}^{j-1} L_p}^{\sum_{p=1}^j L_p} \int_{y_m}^{y_{m+1}} \frac{(k' - k'_0)(s, t) e^{ik[(a_j \sin\theta - b_j \cos\theta)t - \sigma_m s]}}{\sqrt{(y_{m+1} - y_m)}} ds dt \\ R_5 &= 2 \sum_{j=n_s+1}^n (1 - R_k) [b_j \cos\theta + a_j \sin\theta] e^{ik(c_j \sin\theta - d_j \cos\theta)} \int_{\sum_{p=1}^{j-1} L_p}^{\sum_{p=1}^j L_p} \int_{y_m}^{y_{m+1}} \frac{(s - s_0)(s, t) e^{ik[(a_j \sin\theta - b_j \cos\theta)t - \sigma_m s]}}{\sqrt{(y_{m+1} - y_m)}} ds dt \\ R_6 &= 2 \sum_{j=n_s+1}^n (1 + R_k) e^{ik(c_j \sin\theta - d_j \cos\theta)} \int_{\sum_{p=1}^{j-1} L_p}^{\sum_{p=1}^j L_p} \int_{y_m}^{y_{m+1}} \frac{(t_0 - t)(s, t) e^{ik[(a_j \sin\theta - b_j \cos\theta)t - \sigma_m s]}}{\sqrt{(y_{m+1} - y_m)}} ds dt \end{aligned}$$

Thus we need to evaluate the following double integrals, where we let  $y_j = \sum_{p=1}^{j-1} L_p$ ,  $y_{j+1} = \sum_{p=1}^j L_p$  and  $\sigma_j = a_j \sin\theta - b_j \cos\theta$ .

$$\begin{aligned} I_{m,j}^3 &= \int_{y_j}^{y_{j+1}} \int_{y_m}^{y_{m+1}} \frac{(k_0 - k)(s, t) e^{ik(\sigma_j t - \sigma_m s)}}{\sqrt{(y_{m+1} - y_m)}} ds dt \\ I_{m,j}^4 &= \int_{y_j}^{y_{j+1}} \int_{y_m}^{y_{m+1}} \frac{(k' - k'_0)(s, t) e^{ik(\sigma_j t - \sigma_m s)}}{\sqrt{(y_{m+1} - y_m)}} ds dt \\ I_{m,j}^5 &= \int_{y_j}^{y_{j+1}} \int_{y_m}^{y_{m+1}} \frac{(s - s_0)(s, t) e^{ik(\sigma_j t - \sigma_m s)}}{\sqrt{(y_{m+1} - y_m)}} ds dt \\ I_{m,j}^6 &= \int_{y_j}^{y_{j+1}} \int_{y_m}^{y_{m+1}} \frac{(t_0 - t)(s, t) e^{ik(\sigma_j t - \sigma_m s)}}{\sqrt{(y_{m+1} - y_m)}} ds dt \end{aligned}$$

These integrals are similar to those we evaluated for the left hand side, except that  $y_j$  and  $y_{j+1}$

are the two end-points of the side  $\Gamma_j$ , rather than the support of the basis function  $\rho_j$ , and  $\sigma_j = a_j \sin \theta - b_j \cos \theta$ , not  $\pm 1$ . There is also a factor of  $\sqrt{(y_{j+1} - y_j)}$  missing from the denominator in each integrand, and the order of integration is reversed. Evaluation is by Gaussian quadrature as before.

For  $l = j$ ,  $I_{m,j}^3$  and  $I_{m,j}^4$  equal zero, since  $(k_0 - k)(s, t) = (k' - k'_0)(s, t)$ , while  $I_{m,j}^6$  has a reduced kernel as for  $L_5$ .  $I_{m,j}^5$  is evaluated analytically in the same fashion as  $L_4$ .

$$\begin{aligned} I_{m,j}^5 &= \int_{y_j}^{y_{j+1}} \int_{y_m}^{y_{m+1}} \left[ \frac{i-2i}{4} \frac{1}{\pi} \int_0^\infty \frac{e^{(i-r)k|s-t|} - e^{(i-r)k_0|s-t|}}{r^{\frac{1}{2}}(r-2i)^{\frac{1}{2}}} dr \right] \frac{e^{ik(\sigma_j t - \sigma_m s)}}{\sqrt{(y_{m+1} - y_m)}} ds dt \\ &= \frac{1}{2\pi \sqrt{(y_{m+1} - y_m)}} \int_0^\infty \frac{J(r)}{r^{\frac{1}{2}}(r-2i)^{\frac{1}{2}}} dr \end{aligned} \quad (4.10)$$

We again make the substitution  $r = \frac{s^2}{1-s^2}$  to remove the singularity at  $r = 0$ , and evaluate  $J(r)$  as follows

$$J(r) = \int_{y_j}^{y_{j+1}} \int_{y_m}^{y_{m+1}} e^{(i-r)k|s-t| + ik(\sigma_j t - \sigma_m s)} - e^{(i-r)k_0|s-t| + ik(\sigma_j t - \sigma_m s)} ds dt$$

Using the same approach as for  $L_5$ , we obtain

$$\begin{aligned}
J(r) &= \left[ \frac{e^{((i-r)k-ik\sigma_m)x_{m+1}} - e^{((i-r)k-ik\sigma_m)x_m}}{(i-r)k - ik\sigma_m} \right] \left[ \frac{e^{((r-i)k+ik\sigma_j)x_m} - e^{((r-i)k+ik\sigma_j)y_j}}{(r-i)k + ik\sigma_j} \right] \\
&- \left[ \frac{e^{((i-r)k_0-ik\sigma_m)x_{m+1}} - e^{((i-r)k_0-ik\sigma_m)x_m}}{(i-r)k_0 - ik\sigma_m} \right] \left[ \frac{e^{((r-i)k_0+ik\sigma_j)x_m} - e^{((r-i)k_0+ik\sigma_j)y_j}}{(r-i)k_0 + ik\sigma_j} \right] \\
&+ \left[ \frac{e^{((r-i)k-ik\sigma_m)x_{m+1}} - e^{((r-i)k-ik\sigma_m)x_m}}{(r-i)k - ik\sigma_m} \right] \left[ \frac{e^{((i-r)k+ik\sigma_j)y_{j+1}} - e^{((i-r)k+ik\sigma_j)x_{m+1}}}{(i-r)k + ik\sigma_j} \right] \\
&- \left[ \frac{e^{((r-i)k_0-ik\sigma_m)x_{m+1}} - e^{((r-i)k_0-ik\sigma_m)x_m}}{(r-i)k_0 - ik\sigma_m} \right] \left[ \frac{e^{((i-r)k_0+ik\sigma_j)y_{j+1}} - e^{((i-r)k_0+ik\sigma_j)x_{m+1}}}{(i-r)k_0 + ik\sigma_j} \right] \\
&+ \frac{1}{(r-i)k - ik\sigma_m} \left[ \frac{e^{(ik(\sigma_j-\sigma_m))x_{m+1}} - e^{(ik(\sigma_j-\sigma_m))x_m}}{ik(\sigma_j - \sigma_m)} - \frac{e^{(r-i)k(x_m-x_{m+1})+ik(\sigma_j x_{m+1}-\sigma_m x_m)} - e^{ik(\sigma_j-\sigma_m)x_m}}{(i-r)k + ik\sigma_j} \right] \\
&- \frac{1}{(r-i)k_0 - ik\sigma_m} \left[ \frac{e^{(ik(\sigma_j-\sigma_m))x_{m+1}} - e^{(ik(\sigma_j-\sigma_m))x_m}}{ik(\sigma_j - \sigma_m)} - \frac{e^{(r-i)k_0(x_m-x_{m+1})+ik(\sigma_j x_{m+1}-\sigma_m x_m)} - e^{ik(\sigma_j-\sigma_m)x_m}}{(i-r)k_0 + ik\sigma_j} \right] \\
&- \frac{1}{(i-r)k - ik\sigma_m} \left[ \frac{e^{(ik(\sigma_j-\sigma_m))x_{m+1}} - e^{(ik(\sigma_j-\sigma_m))x_m}}{ik(\sigma_j - \sigma_m)} - \frac{e^{ik(\sigma_j-\sigma_m)x_{m+1}} - e^{(r-i)k(x_m-x_{m+1})+ik(\sigma_j x_m-\sigma_m x_{m+1})}}{(r-i)k + ik\sigma_j} \right] \\
&+ \frac{1}{(i-r)k_0 - ik\sigma_m} \left[ \frac{e^{(ik(\sigma_j-\sigma_m))x_{m+1}} - e^{(ik(\sigma_j-\sigma_m))x_m}}{ik(\sigma_j - \sigma_m)} - \frac{e^{ik(\sigma_j-\sigma_m)x_{m+1}} - e^{(r-i)k_0(x_m-x_{m+1})+ik(\sigma_j x_m-\sigma_m x_{m+1})}}{(r-i)k_0 + ik\sigma_j} \right]
\end{aligned}$$

### 4.3 Gaussian quadrature

We have encountered many integrals that we cannot evaluate analytically, so we use Gaussian quadrature. Gaussian quadrature is a method of numerically approximating a definite integral by taking the weighted sum of the function value at a set of given nodes. ie

$$\int_{-1}^1 g(y)dx \approx \sum_{i=1}^{n_q} w_i g(y_i)$$

where we have  $n_q$  nodes at the points  $y_i$  with corresponding weights  $w_i$ . For  $n_q$  quadrature points, the method yields an exact result for polynomials of degree  $2n - 1$ . The integrals we encounter cover some interval  $[a, b]$ , so we transform the weights and nodes to an integral over  $[-1, 1]$ , which is the standard interval for Gaussian quadrature

$$\begin{aligned} w_i &\rightarrow w_i \times \frac{b-a}{2} \\ y_i &\rightarrow a + (b-a) \frac{(y_i+1)}{2} \end{aligned}$$

We have encountered two types of integral that we must approximate numerically, and we will briefly discuss how we apply the method of Gaussian quadrature in each case.

#### 4.3.1 1-D non-oscillatory integrals

These are integrals of the form (4.4) and (4.10). After substitution, we evaluate with 100 quadrature points. This should produce a close approximation due to the non-oscillatory nature of the integral.

#### 4.3.2 2-D oscillatory integrals

Every integral that does not fall into the previous category, we classify as a 2-D oscillatory integral. To begin, there is the obvious complication that we have only looked at approximating 1-D integrals. We carry out a 2-D quadrature as follows. We have the double integral

$$I = \int_a^b \int_c^d g(s, t) dt ds$$

We first compute an approximation to the inner integral,  $h(s) = \int_c^d g(s, t) dt$  for  $s_i, i = 1, \dots, n_t$

$$h_{approx} = \sum_{i=1}^{n_t} w_i^t g(s_i, t_i)$$

and then approximate the outer integral using  $h_{approx}$

$$I_{approx} = \sum_{i=1}^{n_s} w_i^s h_{approx}(s_i)$$

where  $n_s$  and  $n_t$  are the number of quadrature points we use in the  $s$  and  $t$  directions. There are two points to note here. Firstly, we require nodes in both directions, so we expect the quadrature to be

computationally expensive. Specifically, if we want to double the number of nodes in each direction, we end up with four times as many in total.

Secondly, we have said that these integrals are oscillatory (we expect that the wavelength is much smaller than the support of the basis functions), and we would expect the oscillation to be of the order of the incident wavelength. As  $k$  increases the integral becomes increasingly oscillatory. We cannot approximate these integrals accurately using a quadrature method, so we sub-divide the intervals such that the smaller intervals are of order one wavelength in each direction. This removes the oscillatory nature of the integrand on the sub-interval, and we can use Gaussian quadrature to obtain an accurate value for the integral there. On each interval then, we place  $N_s$  equally spaced nodes in the  $s$  direction, and  $N_t$  in the  $t$  direction, and evaluate using  $N_q$  quadrature points.

We have the additional problem that the integrals tend to be highly peaked or singular when the basis functions are very close and  $R$  is very small. This is easily seen in the integrands, since we have terms like  $H_0^{(1)}(z)$ ,  $H_1^{(1)}(z)$  and  $H_2^{(1)}(z)$ , which are undefined at zero.  $R$  is zero or very small in two instances; when the basis functions are on different sides but close to the same corner; and when the basis functions overlap or coincide on the same side (figure 4.1).

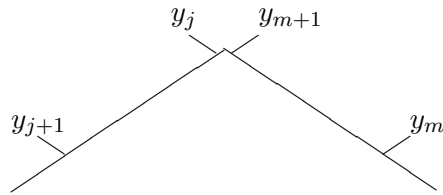


Figure 4.2: Basis functions near the same corner

We overcome this problem by further sub-dividing the interval where we have the singularity or peak. We use a graded mesh on the interval  $[a, a+h_s] \times [c, c+h_t]$ , where  $(a, c)$  is the location of the peak or singularity. We place  $n_q$  nodes at  $a + 0.15^i h_s$  and  $c + 0.15^i h_t$ , for  $i = 1, \dots, n_q$ .  $n_q$  is determined by the proximity of the basis functions. If  $R = 0$ ,  $n_q = N_q$ , so that we use the same number of quadrature points on the graded mesh as we do on each standard interval. If  $R \neq 0$ , then  $n_q$  is chosen such that

$0.15^{n_q}$  is the minimum of  $a$  or  $c$ . The graded 2-D mesh is illustrated below. Note that it is not to scale (the actual mesh is very highly graded towards  $(a, c)$ ) in order to clarify the sub-division of the interval.

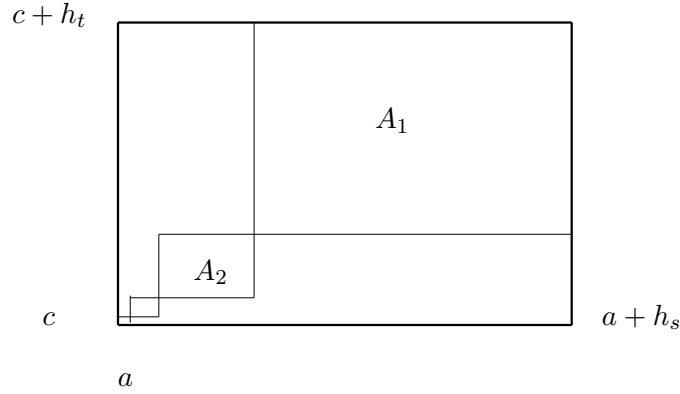


Figure 4.3: Graded mesh near a singularity or peak

The original integral is changed to individual integrals over  $A_1, A_2, \dots, A_{n_q+1}$ . As  $n_q$  increases, the nodes become highly concentrated near  $(a, c)$ , which is exactly what we require to obtain an accurate approximation to the integral on  $[a, a + h_s] \times [c, c + h_t]$

## 5 Numerical Results

### 5.1 Reproducing an acoustic scattering problem

Our first task is to reproduce the acoustic scattering results in [6]. In the limit  $\sigma \rightarrow \infty$ , the transmission problem becomes an exterior scattering problem with  $u^t = 0$  on  $\Gamma$ . We give  $k_0$  an arbitrarily high imaginary component ( $10^{21}i$ ), to mimic this. We set  $k = 4, \theta = \pi/4$  for  $N = 128$ . The scatterer is a square of side  $\pi$ . Figure 5.1 gives total and diffracted field plots for our approximation and the original result, while figure 5.2 shows plots of  $|\varphi|$  and  $|\varphi_{\partial u/\partial n}|$  on the boundary, where we would expect  $|\varphi_{\partial u/\partial n}|$

to approximate  $|\varphi|$  well.

At first glance the approximation is not too bad. The field inside is zero and it models the reflected wave and shadow zone well. The diffracted fields are also qualitatively similar. However, figure 5.2 shows that  $|\varphi_{\partial u/\partial n}|$  is several orders of magnitude higher than  $|\varphi|$ , when we would expect the two to be similar.

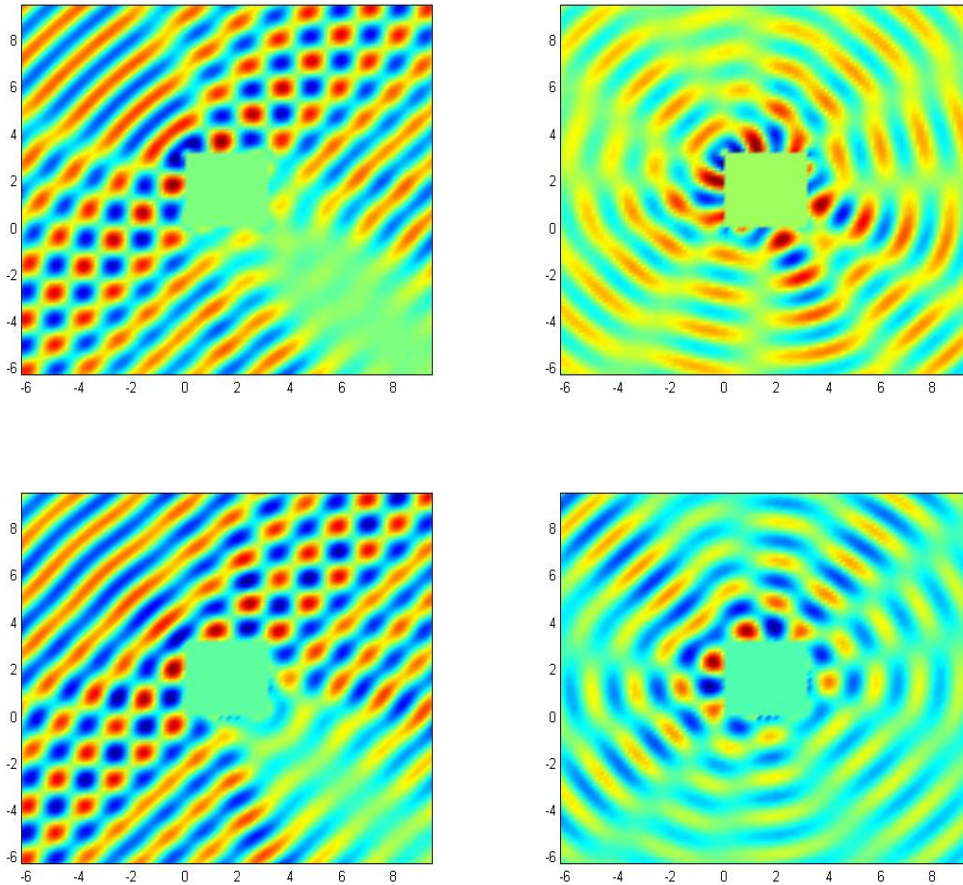
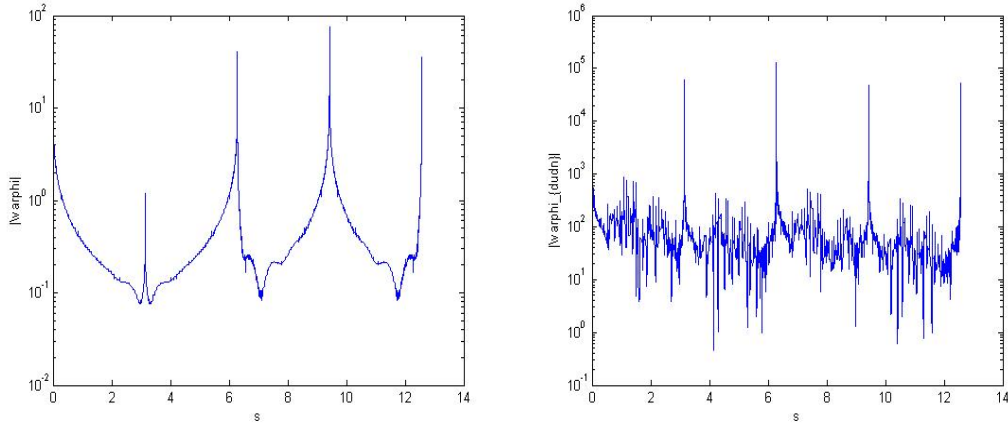


Figure 5.1: Total (left) and diffracted (right) fields for an acoustic scattering problem,  $k = 4, \theta = \pi/4, N = 128$ . Original result (top), our approximation (bottom)

Figure 5.2:  $|\varphi|$  (left) and  $|\varphi_{\partial u / \partial n}|$  (right) on the boundary

## 5.2 Acoustic scattering problem without subtraction of the leading order behaviour

We consider the acoustic scattering problem (2.12) (square of side  $2\pi$ ), for wavenumber  $k = 10$ , and solve it without subtracting the leading order behaviour, so that we approximate  $\partial u^s / \partial n$  directly. We take the exact solution to be that obtained when we do subtract the leading order behaviour, for  $N = 64$ . Table 5.1 gives the relative  $L^2$  errors, and figure 5.3 shows the total field for each value of  $N$ . We compare these to figure 5.4, the field obtained from subtracting the leading order behaviour, for  $N = 64$ . In this case then, we have not subtracted the leading order behaviour and still obtained the correct result.

$N$	Relative $L_2$ error
8	$3.2440 \times 10^0$
16	$6.7612 \times 10^0$
32	$5.669 \times 10^{-1}$
64	$2.010 \times 10^{-1}$

Table 5.1: Relative  $L_2$  errors for acoustic case where there is no subtraction

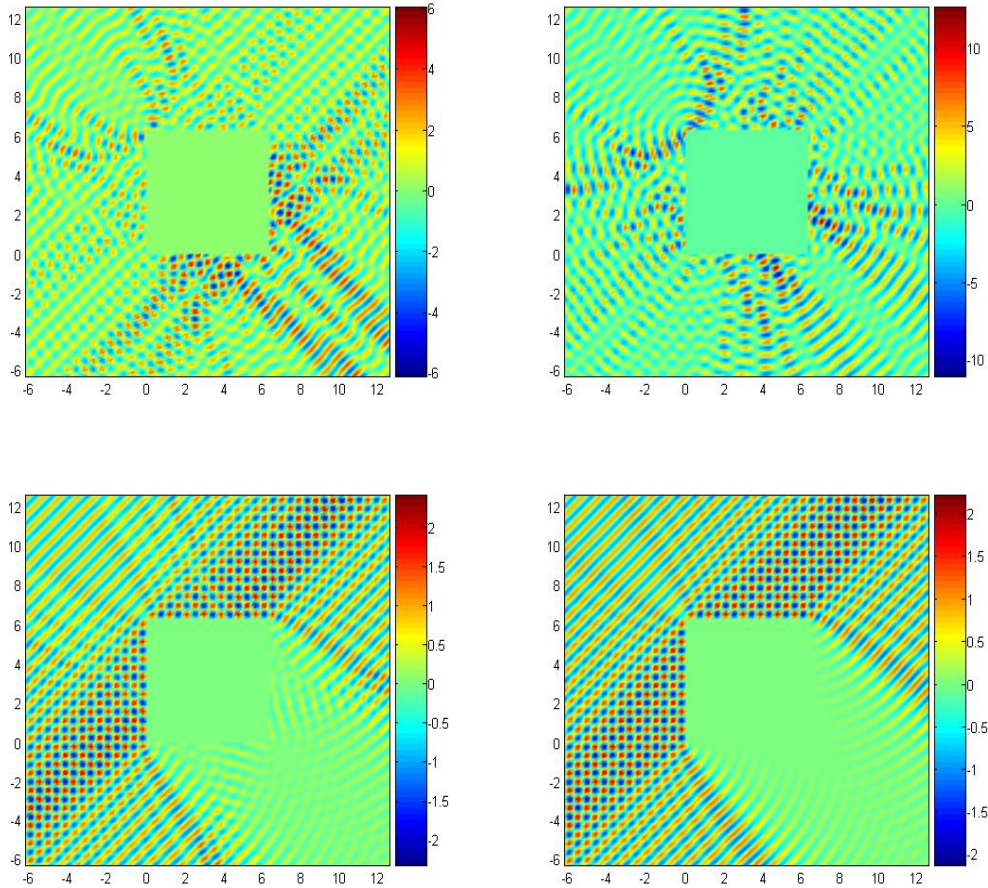


Figure 5.3: Acoustic scattering without subtraction of leading order behaviour,  $N=8,16,32,64$

### 5.3 Transmission through a hexagonal ice crystal

We now consider transmission through a unit hexagonal ice crystal, side length 1. We use  $n_{ice} = 1.31 + 0.01i$ , with an incident wavenumber of 20 and angle of incidence  $\theta = 49\pi/100$ . We plot the total and transmitted fields for values of  $N = 2, 4, 8, 16, 32$  and 64 (figures 5.5 and 5.6). The transmitted field is the total field minus the incident and reflected components, and is the part of the field that we approximate by  $\varphi_u$  and  $\varphi_{\partial u/\partial n}$ . We also plot  $|\varphi_u|$  and  $|\varphi_{\partial u/\partial n}|$  on the boundary for  $N = 32, 64$  and 128 (figure 5.7).

We obtain promising results, although we cannot say with any certainty whether we are approxi-

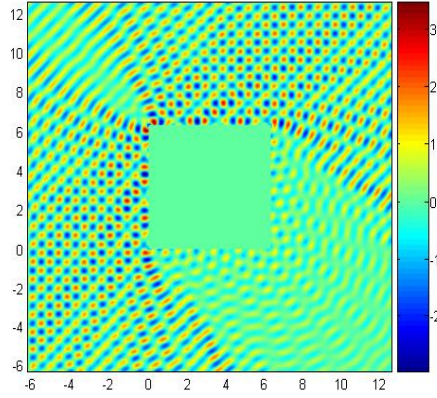


Figure 5.4: Acoustic scattering with subtraction of leading order behaviour,  $k=10$ ,  $N=64$

imating the true solution or not. We expect that the the incident wave will be well transmitted through the ice crystal, since it is not very attenuating. We observe that the transmitted field and its normal derivative oscillate on the boundary and have approximately the same amplitude across the boundary (figure 5.7), with peaked behaviour at the corners. For the two largest values of  $N$ , 32 and 64, there appears to be convergence towards the same solution, visible in both the plots on the boundary (particularly  $|\varphi_{\partial u/\partial n}|$ ) and the total and transmitted field plots.

It is a well known phenomena that cylindrical ice crystals with a hexagonal cross-section give rise to a 22 degree halo. This is often observed when light from the moon or sun is refracted by ice crystals associated with thin, high-level clouds. It is difficult to say whether we observe this effect.

#### 5.4 Transmission through a triangular ice crystal

We now look at transmission through an equilateral triangular ice crystal, side length  $\pi$ , with wavenumber  $k = 4$  and  $\theta = \pi/3$ . This time we neglect absorption, so the wavenumber inside is real, and  $k_0 = 1.31 * k = 5.24$ . Figure 5.8 shows plots of the total and transmitted fields for  $N = 16, 32, 64$  and 128. Figure 5.9 plots  $|\varphi_u|$  and  $|\varphi_{\partial u/\partial n}|$  on the boundary for  $N = 32, 64$  and 128. As  $N$  increases there is a definite convergence of  $|\varphi_u|$  and  $|\varphi_{\partial u/\partial n}|$  on the boundary, particularly so for the latter.

Taking the  $N = 128$  values  $\varphi_{u_{128}}$  and  $\varphi_{\partial u/\partial n_{128}}$  as the true solution, we compute the relative  $L^2$

errors for  $N = 2, 4, 8, 16, 32$  and  $64$  in table 5.2.

### 5.5 Transmission through a thin strip

Figure 5.10 shows plots of the total and transmitted field for an incident field ( $k = 20, \theta = 49\pi/100$ ) on a rectangular strip with dimensions 1 by 10. Inside  $k_0 = 34 + 5i$ . We see very clear features; a partially reflected wave interacting with the incident wave; diffraction at either end of the strip giving rise to noticeable interference patterns in the shadow zone behind the obstacle; and a travelling wave inside the strip that is attenuated relatively strongly.

## 6 Conclusions and Further Work

We have adapted a Galerkin boundary element method for acoustic scattering and applied it to an electromagnetic transmission problem.

We have obtained encouraging results, but it is clear that this particular Galerkin boundary element method does not suit this particular problem. We have seen (for example figure 5.7) that in the transmission case,  $u^t$  and its normal derivative have an amplitude which is approximately constant across the boundary. This is exactly what we might expect for a medium which attenuates transmitted waves by only a small amount. We do expect that the field on the boundary will be peaked at the corners, but not to the same extent that it occurs in [6], so a more standard mesh (ie less grading) might be more appropriate for the problem.

A key avenue of investigation would be to identify the leading behaviour on shadow sides, for the transmission problem. Only when we know how the field behaves on the boundary, can we be confident that a given method will work. Plus, we might then design a mesh specifically for this problem. We might also use a collocation or an hp boundary element scheme, rather than a Galerkin one. In [2], it is shown that the collocation method converges to the same solution as the Galerkin scheme with a lower computational cost. We also recall that we have utilised piecewise constants in our basis functions. Using piecewise polynomials of degree  $\geq 1$  should produce a better rate of convergence.

We stated in the introduction that our aim was “to investigate the extent to which the numerical

solution of electromagnetic scattering problems can be enhanced using methods developed for acoustic scattering”, with reference to the Galerkin scheme we have implemented. Despite a lack of tangible results, this method has showed decent promise and further work in this area should prove to be worthwhile.

## References

- [1] M. ABRAMOWITZ AND I. STEGUN, *Handbook of Mathematical Functions*, Dover, 1972.
- [2] S. ARDEN, S. N. CHANDLER-WILDE AND S. LANGDON, *A collocation method for high frequency scattering by convex polygons*, to appear in *J. Comp Appl. Math.*
- [3] A. BARAN, UK METEOROLOGICAL OFFICE, *private communication*
- [4] S. N. CHANDLER-WILDE, *Boundary value problems for the Helmholtz equation in a half-plane*, in *Proc. 3rd Int. Conf. on Mathematical and Numerical Aspects of Wave Propagation*, G. Cohen, ed., SIAM, Philadelphia, 1995.
- [5] D. COLTON AND R. KRESS, *Integral Equation Methods in Scattering Theory*, Wiley, 1983.
- [6] S. LANGDON AND S. N. CHANDLER-WILDE, *A Galerkin Boundary Element Method for High Frequency Scattering by Convex Polyons*
- [7] S. LANGDON AND S. N. CHANDLER-WILDE, *Implementation of a boundary element method for high frequency scattering by convex polygons*, in *Advances in Boundary Integral Methods (Proceedings of the 5th UK Conference on Boundary Integral Methods)*, K. Chen, ed., Liverpool University Press, 2005, pp. 2–11.
- [8] —, *A wavenumber independent boundary element method for an acoustic scattering problem*, *SIAM J. Numer. Anal.*, 43 (2006), pp. 2450–2477.
- [9] F. OBERHETTINGER AND L. BADI, *Tables of Laplace Transforms*, Springer-Verlag, 2005

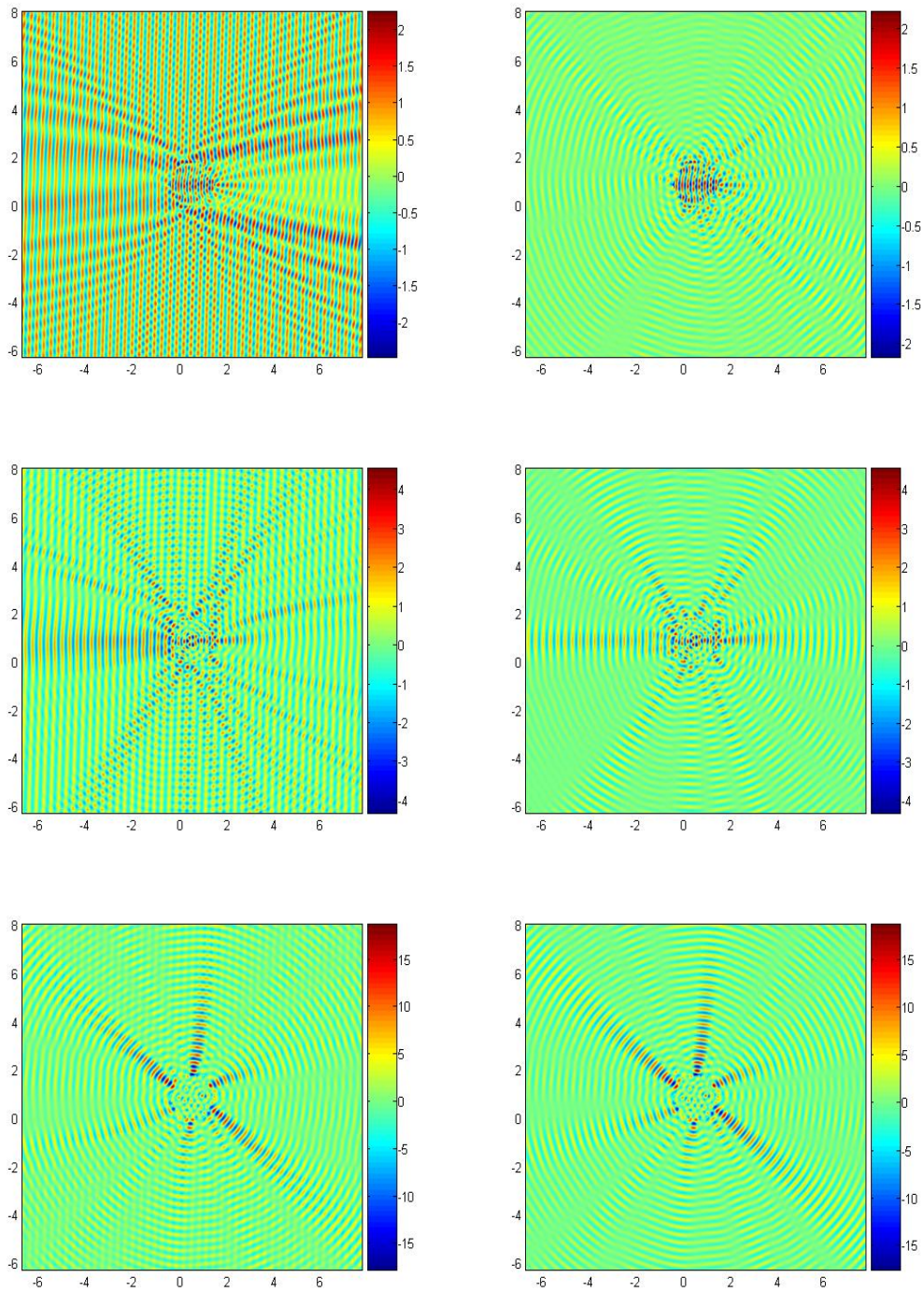


Figure 5.5: Total (left) and transmitted (right) fields for transmission through a hexagon,  $k = 20$ ,  $\theta = 49\pi/100$ ,  $N = 2, 4, 8$

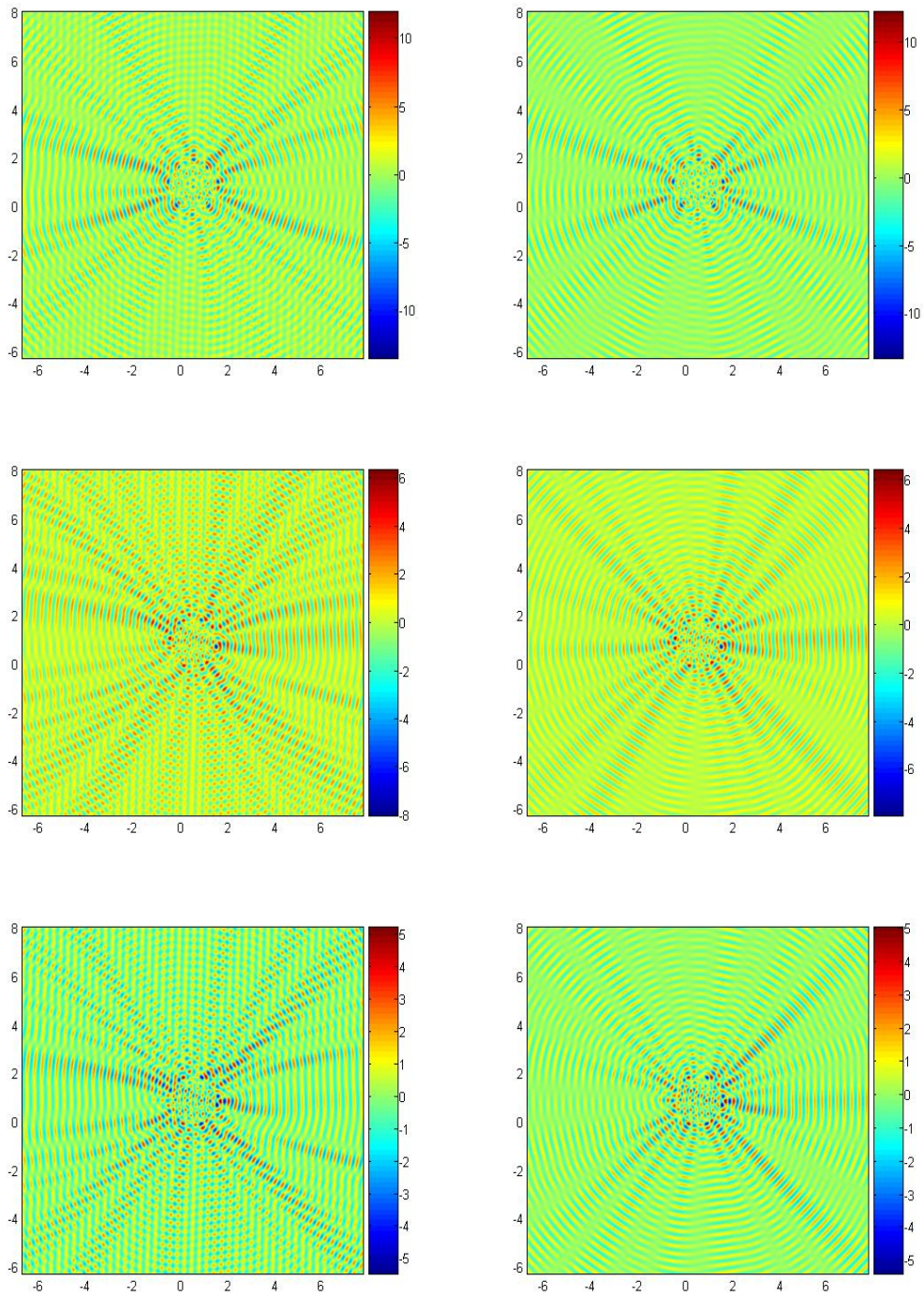


Figure 5.6: Total (left) and transmitted (right) fields for transmission through a hexagon,  $k = 20$ ,  $\theta = 49\pi/100$ ,  $N = 16, 32, 64$

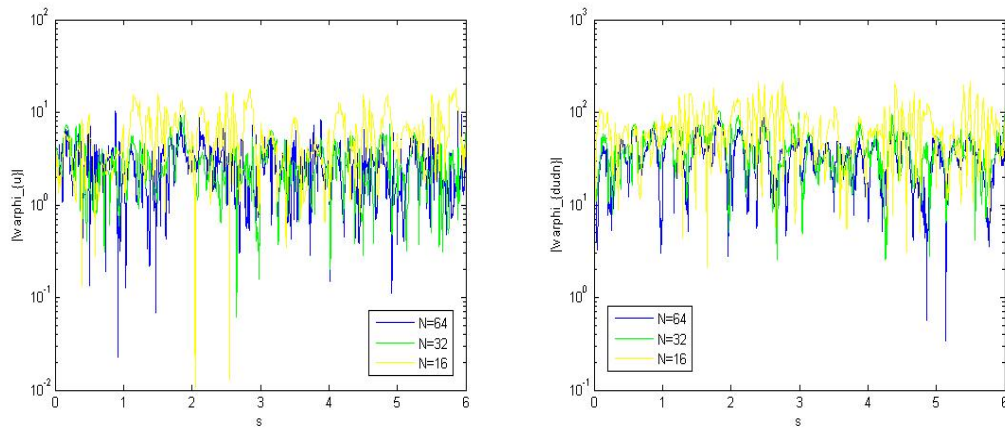


Figure 5.7: Plots of  $|\varphi_u|$  (left) and  $|\varphi_{\partial u/\partial n}|$  (right) on the boundary of the hexagon

$N$	Relative $L^2$ error $\varphi_u$	Relative $L^2$ error $\varphi_{\partial u/\partial n}$
2	$4.0397 \times 10^0$	$3.5475 \times 10^0$
4	$6.2566 \times 10^0$	$5.5322 \times 10^0$
8	$1.0164 \times 10^0$	$1.3859 \times 10^0$
16	$9.108 \times 10^{-1}$	$1.6887 \times 10^0$
32	$1.0020 \times 10^0$	$8.262 \times 10^{-1}$
64	$8.691 \times 10^{-1}$	$3.284 \times 10^{-1}$

Table 5.2: Relative L2 errors for trianlge case

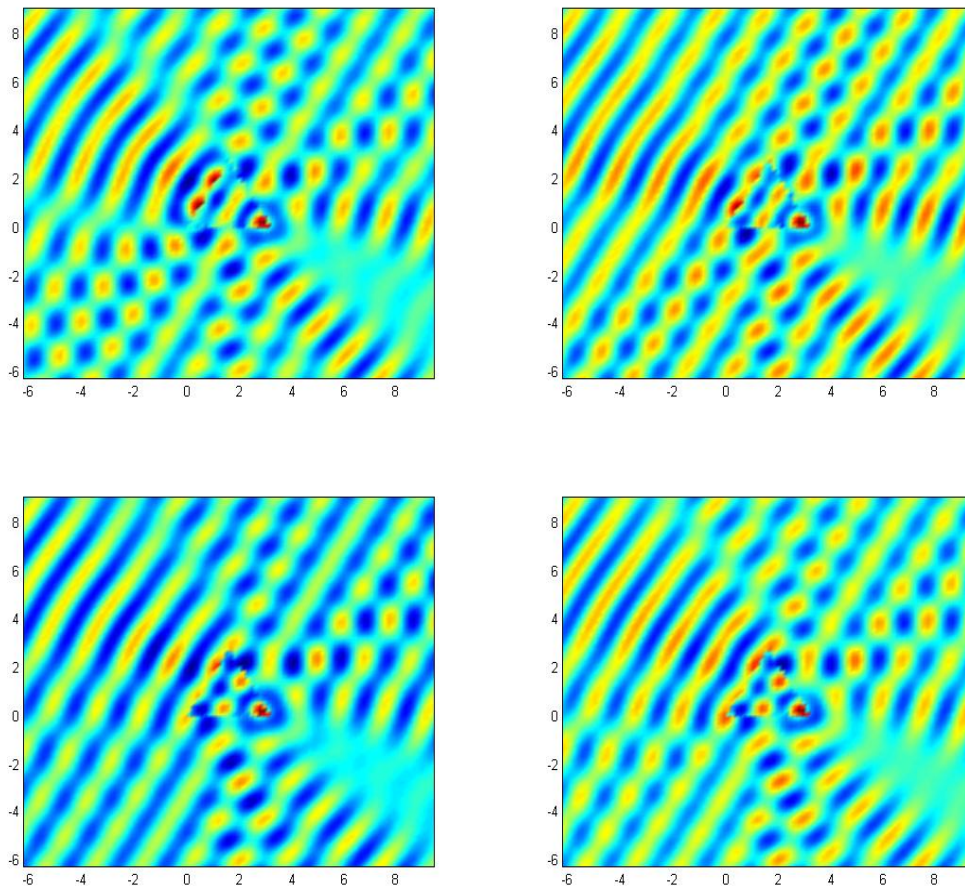


Figure 5.8: Total field plotted for transmission through a triangle,  $k = 4, \theta = \pi/3, N = 16$  (top left),  $N = 32$  (top right),  $N = 64$  (bottom left) and  $N = 128$  (bottom right)

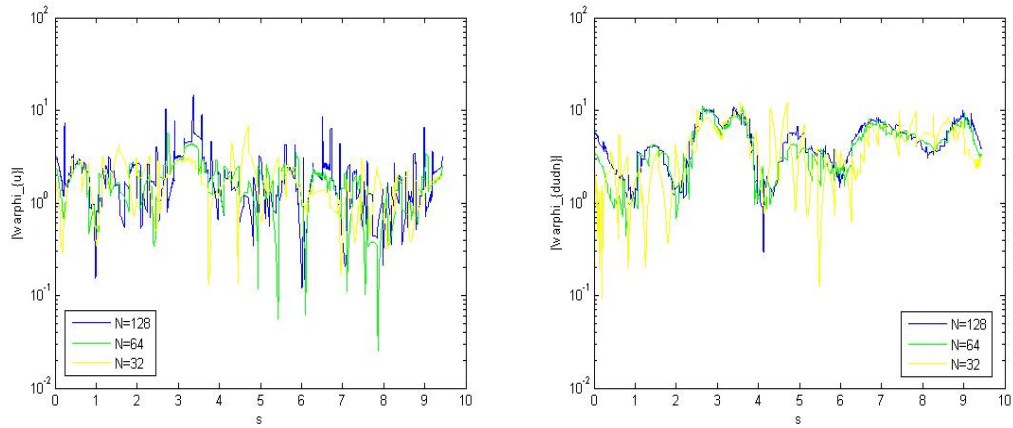


Figure 5.9: Plots of  $|\varphi_u|$  and  $|\varphi_{\partial u / \partial n}|$  on the boundary of the triangle

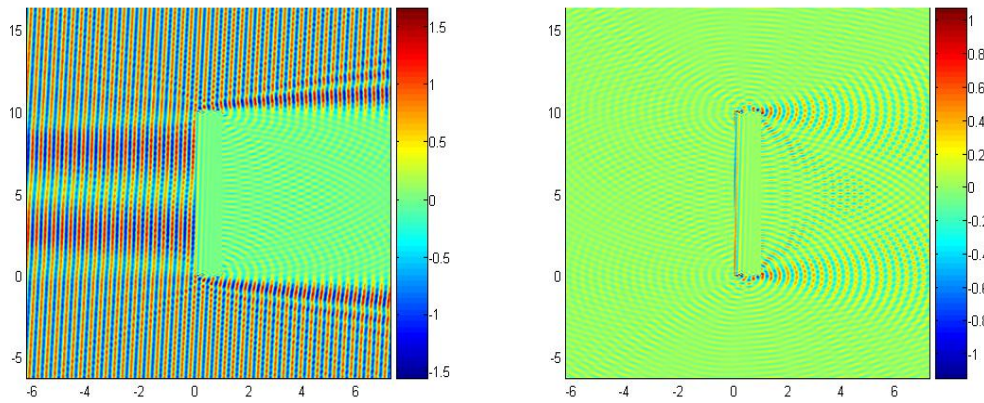


Figure 5.10: Total and transmitted fields for transmission through a thin strip